

Spectral regularization for adversarially-robust representation learning

Sheng Yang^{*1}, Jacob A. Zavatone-Veth^{+1,2,3}, and Cengiz Pehlevan^{‡1,2,4}

¹*John A. Paulson School of Engineering and Applied Sciences, Harvard University, Cambridge, MA*

²*Center for Brain Science, Harvard University, Cambridge, MA*

³*Department of Physics, Harvard University, Cambridge, MA*

⁴*Kempner Institute for the Study of Natural and Artificial Intelligence, Harvard University, Cambridge, MA*

May 28, 2024

Abstract

The vulnerability of neural network classifiers to adversarial attacks is a major obstacle to their deployment in safety-critical applications. Regularization of network parameters during training can be used to improve adversarial robustness and generalization performance. Usually, the network is regularized end-to-end, with parameters at all layers affected by regularization. However, in settings where learning representations is key, such as self-supervised learning (SSL), layers after the feature representation will be discarded when performing inference. For these models, regularizing up to the feature space is more suitable. To this end, we propose a new spectral regularizer for representation learning that encourages black-box adversarial robustness in downstream classification tasks. In supervised classification settings, we show empirically that this method is more effective in boosting test accuracy and robustness than previously-proposed methods that regularize all layers of the network. We then show that this method improves the adversarial robustness of classifiers using representations learned with self-supervised training or transferred from another classification task. In all, our work begins to unveil how representational structure affects adversarial robustness.

1 Introduction

Neural networks are vulnerable to adversarial attacks [1, 2]. For classification tasks, an originally correctly-classified sample may be recognized incorrectly after adding a perturbation so small as to be imperceptible to the human eye [2, 3]. Even without access to the model parameters and only access to inputs and outputs, attackers can still fool the network [4–6]. Identifying effective training algorithms that guard against these black-box attacks has therefore garnered widespread attention in the last decade [4, 7, 7–11]. Developing training mechanisms that provably provide black-box adversarial robustness is thus crucial in the development of practically deployable machine learning.

^{*}shengyang@g.harvard.edu

[†]jzavatoneveth@g.harvard.edu

[‡]cpehlevan@seas.harvard.edu

However, recent years have seen growing popularity of representation learning paradigms to which many previous adversarial defenses are not immediately applicable. For instance, in transfer learning and self-supervised learning, the final linear readout layer of a network is retrained when performing downstream inference tasks. Only layers up to the feature representations are kept from the pretraining stage [12–15]. As standard adversarial training methods for classification networks typically require access to the last layer linear heads [16, 17], they cannot be directly applied in representation learning settings.

In this paper, we seek an adversarial training methodology that can be applied to these representation-focused training paradigms, in which the representation is pre-trained without knowledge of downstream tasks. Our primary contributions are organized as follows: We begin by introducing relevant previous works in Section 2. Then, in Section 3, we derive a theoretical guarantee on black-box adversarial robustness based on feature representations. This bound inspires our proposed regularizer Equation (5), which penalizes the top singular value of each hidden layer’s weights (i.e. excluding the last layer’s linear head). In Section 4, we empirically demonstrate the effectiveness of this regularizer. We first show that it enlarges adversarial distances even more than regularizers incorporating the last layer for end-to-end classification training. Then, we show that it improves both adversarial robustness and test accuracy in both self-supervised and transfer learning across a range of simulated and moderate-scale image classification tasks. Our results provide evidence that having robust representations is crucial to adversarial robustness.

2 Related Works

This section provides a brief overview of the adversarial robustness literature, with a focus on black-box defenses. Two major approaches to improve black-box adversarial robustness have been proposed: training with adversarial examples and regularization [5, 18]. To train with adversarial samples, in each update to the network parameters, the training set is augmented with adversarial examples. Since we have access to input gradients during model training, one can use white-box attacks to find these examples [3, 4, 6–11]. By forcing the model to become robust to these perturbations during training, it becomes less susceptible to future adversarial attacks.

However, training with adversarial examples is computationally expensive, and it does not guarantee that the final classifier will be adversarially robust because of its strong dependence on the training dataset [16]. A less data-dependent and more computation friendly method is to design regularizers that encourage robustness. By adding specially designed regularization terms, the model can escape bad, non-robust local minima during optimization [19]. For linear regression, logistic regression, and decision trees with known uncertainty set structure, an exact equivalence between robustness and regularization has been established [20, 21]. In more advanced applications, one can derive regularizers that promote raising lower bounds on the adversarial distance [16, 22, 23]. Our analysis attempts to generalize this adversarial robustness notion further for newer classification architectures.

In either case, searching for an adversarial sample with minimal adversarial distance in a black-box fashion is highly nontrivial. This makes black-box robustness evaluation rather difficult in practice, meaning that it is hard to evaluate defenses conclusively. Many query-based heuristic methods have been proposed [24–30], which rely on iterative search for the closest point on the decision boundary of a trained model to a given sample. In our analysis we employ one such method, the tangent attack (TA) [29], to evaluate model adversarial robustness.

3 Spectral Regularization for Adversarial Robustness

In this section, we build our spectral regularization on representations step-by-step. We first introduce the concept of adversarial distance and adversarial robustness; then we derive a lower bound on adversarial distance based on feature representations inspired by previous work of Hein and Andriushchenko [16]; lastly, we derive the proposed regularizer.

3.1 Preliminaries

We first introduce the notion of black-box adversarial robustness. Consider the problem of assorting n -dimensional data into K given classes. For a classification network $F(x; \Theta) : \mathbb{R}^n \times \mathbb{R}^{|\Theta|} \rightarrow \mathbb{R}^K$ with trainable parameters Θ , the class prediction is given by $\hat{y} = \arg \max_{k \in [K]} F_k(x; \Theta)$, which is correct if it agrees with the true class label y . In the following discussions we drop the Θ notation when there is no ambiguity. Here we assume the output logits are distinct.

Adversarial Perturbation. Consider a perturbation in the input space $\delta_x \in \mathbb{R}^n$ to a correctly-classified sample x . We say δ_x is an adversarial perturbation to x if it swaps the predicted class label, i.e., there is a class index $k \neq y$ such that $F_k(x + \delta_x) > F_y(x + \delta_x)$.

Adversarial Distance. The adversarial distance Δ_x is defined as the minimal size of an adversarial perturbation for the datum x : $\Delta_x = \min_{\{\delta_x \in \mathbb{R}^n : \arg \max_{k \in [K]} F_k(x + \delta_x) \neq y\}} \|\delta_x\|_2$. In this paper we focus on l_2 norm but the analysis can be generalized to other norms as well.

Adversarial Robustness. A network is adversarially robust to input perturbation with respect to sample x if Δ_x is large, and is globally adversarial robust if Δ_x is large for all correctly classified x .

Note that we do not consider perturbing an incorrectly predicted sample. With this objective, past works have observed a tradeoff between adversarial robustness and classification accuracy [2, 3, 31, 32]. We demonstrate this tradeoff through a simple binary classification task in Figure 1. The third scenario is the ideal case, where we reach a globally adversarially robust state. This example motivates us to search for a solution that has large Δ_x for all correctly predicted samples x . Given a desired accuracy level $\rho \in [0, 1]$, define the set of parameters $S_{\rho, D, F}$ for the network F that classifies a dataset $D = \{(x_i, y_i)\}_{i=1}^m$, $(x_i, y_i) \in \mathbb{R}^n \times [K]$ with accuracy at least ρ . Then, we are interested in finding the point within $S_{\rho, D, F}$ that maximizes the minimum adversarial distance:

$$\Theta^{(\text{robust})} = \arg \max_{\Theta \in S_{\rho, D, F}} \min_{i \in [m]} \Delta_{x_i}. \quad (1)$$

In practice, without access to the test set, we hope that having larger adversarial distances in the training set translates to larger distances in the test set, which we validate empirically. The rest of this section thus gives a lower bound on Δ_x using spectral analysis, and derives a regularizer that encourages a neural network to look for parameters that have large such lower bounds.

3.2 A lower bound on adversarial distance

Given a classification network $F(x) : \mathbb{R}^n \rightarrow \mathbb{R}^K$ of L layers, we can decompose it into a feature map $\Phi(x) : \mathbb{R}^n \rightarrow \mathbb{R}^d$, where d is the feature dimension, and a linear decision head $f(z) : \mathbb{R}^d \rightarrow \mathbb{R}^K$:

$$F = \text{SoftMax} \circ f \circ \Phi \quad (2)$$

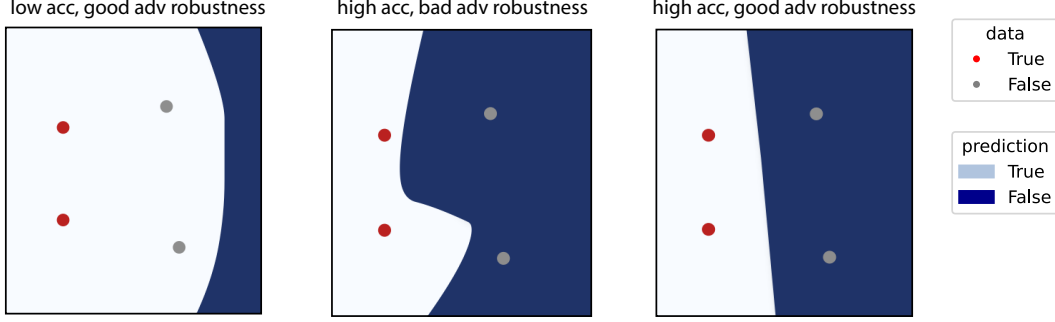


Figure 1: Tradeoff between prediction accuracy and adversarial robustness in a simple binary classification task. The first scenario has 50% accuracy, but the adversarial distances for the correct samples are large. The second case correctly classifies every sample, but does not have large adversarial distances for each. The last scenario is the ideal: a large-margin solution.

With this decomposition, we present our central lemma, which is an extension of the main result of Hein and Andriushchenko [16]. The objective of our analysis is to isolate the influence of the readout weights, as we focus on settings where the representation is learned in a pretraining phase and the readouts are trained separately to perform downstream tasks.

Lemma 1. Suppose a neural network classifier $F : \mathbb{R}^n \rightarrow \mathbb{R}^K$ is continuously differentiable and can be decomposed as Equation (2), with $f(z) = W^{(L)}z$ the last layer linear transformation without bias, and $W_c^{(L)}$ the c -th row of $W^{(L)}$, treated as a row vector. Suppose $x \in \mathbb{R}^n$ is a sample input belonging to class c and $\delta_x \in \mathbb{R}^n$ an adversarial perturbation to x that results in an incorrect prediction of class k . Fixing a perturbation radius ‘budget’ $R > 0$ such that $\|\delta_x\|_2 \leq R$, we have

$$\Delta_x \geq \theta_x \|\Phi(x)\|_2 \cdot \frac{1}{\max_{y \in B_2(x, R)} \|\nabla \Phi(y)\|_2} \quad (3)$$

where $\theta_x = \frac{(W_c^{(L)} - W_k^{(L)})\Phi(x)}{\|W_c^{(L)} - W_k^{(L)}\|_2 \|\Phi(x)\|_2}$ is the cosine of the angle between the feature representation of x and the last layer “confidence weights” $W_c^{(L)} - W_k^{(L)}$ for class c relative to class k . Here, $\nabla \Phi(\cdot)$ is the Jacobian of the feature map with respect to the input.

Proof. See Appendix A.1 for the proof of this lemma, extended to general l_p norms. \square

In this lower bound, the key term of interest from a feature representation perspective is the norm of the feature map’s gradient $\|\nabla \Phi(\cdot)\|_2$ in the denominator. As it depends on the readout weights, the angle θ_x cannot be controlled during the pretraining phase when features are learned. When a readout is subsequently trained to perform a downstream task, θ_x is determined by the algorithm chosen at that stage. We discuss this point, and comment on the dynamics of θ_x in the supervised setting where the readout and representation are learned simultaneously, in Appendix A.3. We also remark that we make the choice to regularize the gradient norm directly rather than explicitly also attempting to control the scale of the representation $\|\Phi(\cdot)\|^2$. This choice is motivated by the fact that a global re-scaling $\Phi(x) \mapsto c \Phi(x)$ could be compensated by downstream readout, while a spatially-anisotropic rescaling will also change the gradient norm.

This lower bound suggests that we should penalize $\max_{y \in B_2(x, R)} \|\nabla \Phi(y)\|_2$ during representation learning. This contrasts with previous works on supervised learning that penalize the input-output Jacobian ∇F [16, 17, 33]. However, to make regularization computationally efficient,

we must make several relaxations of this objective. First, we consider the norm of the gradient at x only, since searching over the whole of the ball is computationally expensive and not easily parallelizable. Noting that the 2-norm of a matrix is its maximum singular value, we have

$$\|\nabla\Phi(x)\|_2^2 = \lambda_{\max}(\nabla\Phi(x)\nabla\Phi(x)^T) = \lambda_{\max}(\nabla\Phi(x)^T\nabla\Phi(x)) =: \lambda_{\max}(g), \quad (4)$$

where we have defined $g := \nabla\Phi(x)^T\nabla\Phi(x)$. Here, $\lambda_{\max}(\cdot)$ denotes the maximum eigenvalue of a matrix. A robust classification network thus must have small $\lambda_{\max}(g)$.

Remark 1. (Metric Tensor) *If we consider Φ as the feature map and pull the Euclidean metric from feature space back to input space, the induced metric tensor is exactly g as defined above. The behavior of the pull-back metrics induced by trained deep network feature maps has been studied by Zavatone-Veth et al. [34], focusing on enlargement of the volume element $\sqrt{\det g}$ near decision boundaries. The conclusion in our work that increasing $\lambda_{\max}(g)$, the dominant term in $\sqrt{\det g}$, encourages adversarial robustness, adds theoretical context to the empirical observations of [34].*

In principle, $\lambda_{\max}(g)$ is differentiable so long as the spectral gap is nonzero, and so can be naively added to the loss term as a regularizer. However, computing the resulting updates using automatic differentiation suffers from high runtime and memory consumption [34]. To alleviate such costs, we perform a series of relaxations. Assuming that the activation function has derivatives (almost everywhere) bounded by 1, we can bound $\lambda_{\max}(g)$ by the product of the largest singular values squared of the hidden layer weights $W^{(l)}$, $\sigma_{\max}^2(W^{(l)})$, where $l \in [L - 1]$ for L the total number of layers. This trick was used before by Yoshida and Miyato [17]. The resulting regularizer, which we henceforth refer to as rep-spectral because it is a spectral regularizer on representations, is

$$L^{(\text{rep-spectral})}(\Theta) = \frac{\gamma}{2} \sum_{l=1}^{L-1} \sigma_{\max}^2(W^{(l)}), \quad (5)$$

where $\gamma \geq 0$ is the regularization strength. We present the full derivation of this regularizer in Appendix A.2. One may use log on the singular values as directly regularizing the product of singular values, but this would incur additional computational costs and result in a data-dependent scaling factors in gradient computation that could be heuristically absorbed in γ . The difference with [17] is that we drop the penalization of the last layer. We refer to their proposed regularizer as ll-spectral to emphasize that it penalizes the top singular value of the readout weights, in contrast to our method. Concretely, their regularizer is

$$L^{(\text{ll-spectral})}(\Theta) = \frac{\gamma}{2} \sum_{l=1}^L \sigma_{\max}^2(W^{(l)}); \quad (6)$$

we will compare the effects of these two regularizers on supervised pretraining in Section 4.

To efficiently compute the parameter update based on this regularization, note that the gradient of the top singular value can be computed analytically under the assumption that it is unique as $\partial\sigma_{\max}^2(W)/\partial W = 2\sigma_{\max}u_{\max}v_{\max}^T$, where u_{\max}, v_{\max} are the left and right singular vectors for σ_{\max} . One can then employ power iterations with singular direction updates amortized across parameter updates [17] instead of automatic differentiation to efficiently adjust the parameters (e.g. perform 1 power iteration every 10 parameter updates when learning rate is small, see Appendix C).

Remark 2. (Extension to Convolutional Neural Networks) *The assumption that F consists of only fully-connected layers can be relaxed. For deep convolutional neural networks, we can compute the maximum singular values of matrix representations of the convolutional layers. Concretely, suppose we are given an input image $X \in \mathbb{R}^{c_{in} \times n \times n}$ and a multi-channel filter $\mathcal{K} \in \mathbb{R}^{c_{out} \times c_{in} \times k \times k}$. Then, there exists a matrix $\tilde{\mathcal{K}} \in \mathbb{R}^{c_{out}n_{out}^2 \times c_{in}n^2}$ such that a periodic 2D convolution can be linearized as $\text{Vec}(\text{Conv2D}(X)) = \tilde{\mathcal{K}} \text{Vec}(X)$, where $\text{Vec}(\cdot)$ is a row-major flattening of the input image X . We can then extract the top eigenvalue of $\tilde{\mathcal{K}}$ for regularization. See details in Appendix B and in [35, 36] for the construction of $\tilde{\mathcal{K}}$ and algorithms to extract its top singular value both exactly and iteratively.*

4 Experiments

We now evaluate our proposed `rep-spectral` regularizer based on the accuracy of classification and the adversarial distance of selected samples at the end of training. For benchmarking purposes and to gain intuition for its effect on pretraining, we first compare it against the `l1-spectral` regularizer in fully supervised settings where there is no separate training. We then turn to the pretraining settings which motivate our work. In all cases, we regard a regularizer to be successful if we observe an increase in average adversarial distances without a significant drop in test accuracy. We will see that there are some cases where the test accuracy in fact improves with regularization.

To evaluate black-box adversarial robustness, we use the Tangent Attack (TA) method [29]. As introduced in Section 2, the TA method seeks an approximation to δ_x , an adversarial perturbation to a correctly classified sample x that is as small as possible in l_2 norm. The TA algorithm uses 2D analytic geometry to iteratively locate the point nearest to x that is assigned a different label by the network (i.e., we focus on non-targeted attacks). We provide a more detailed discussion of the TA method in Appendix D, and document training and evaluation details in Appendix E. Code to reproduce all experiments is available on GitHub.¹

4.1 Shallow MLPs trained on a toy dataset

To gain intuition for how our regularizer shapes representations, we first apply it to a single-hidden-layer MLP trained on a toy 2D XOR task. Though this task is of course unrealistic, it is potentially useful because we can directly visualize the input space. Given 4 data points at $[\pm 1, \pm 1] \in \mathbb{R}^2$, we use a network with 8 hidden units and GELU nonlinearity. Though our regularizer is motivated by the independent-pretraining, we find that even in this fully-supervised setting we obtain improved adversarial robustness, even compared to training using the `l1-spectral` regularizer that penalizes the last layer (Figure 2). More training details and results can be found in Appendix E.1.

How does this robustness arise? As the input space for the XOR task is two-dimensional, we can directly visualize it. Examining the decision boundaries in Figure 3a, we see that our `rep-spectral` regularizer results in increased classification margin, while the `l1-spectral` regularizer does not substantially affect the decision boundary. This difference reflects the fact that `l1-spectral` mostly just penalizes the readout layer norm and fails to control the feature layer norm (Figure E.1). To gain a more detailed understanding of how the representations differ, we visualize the volume element corresponding to the metric induced by the feature map, as described in Remark 1. In Figure 3b, we see that the `rep-spectral` regularizer noticeably increases the areas of small volume element (and thus low representational sensitivity) near the class centers relative to the unregularized and `l1-spectral` models.

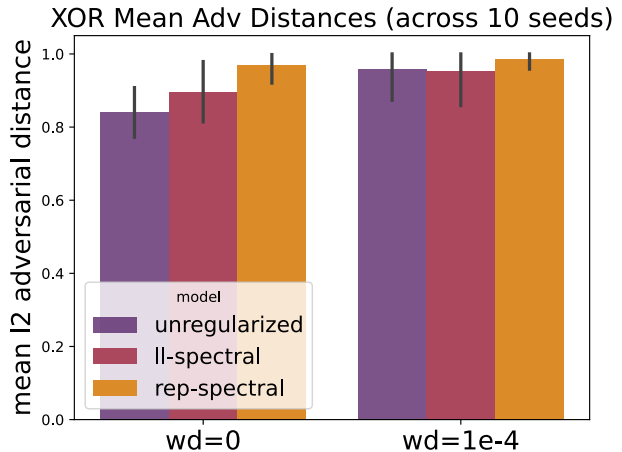


Figure 2: Average Δ_x found by TA across 10 different seeds for models trained on XOR with (*right*) and without (*left*) weight decay, and with the inclusion of our proposed `rep-spectral` regularizer, the `l1-spectral` regularizer that includes all layers, or no additional spectral regularizer. Error bars show ± 1 standard deviation over seeds.

¹<https://github.com/Pehlevan-Group/rep-spectral>

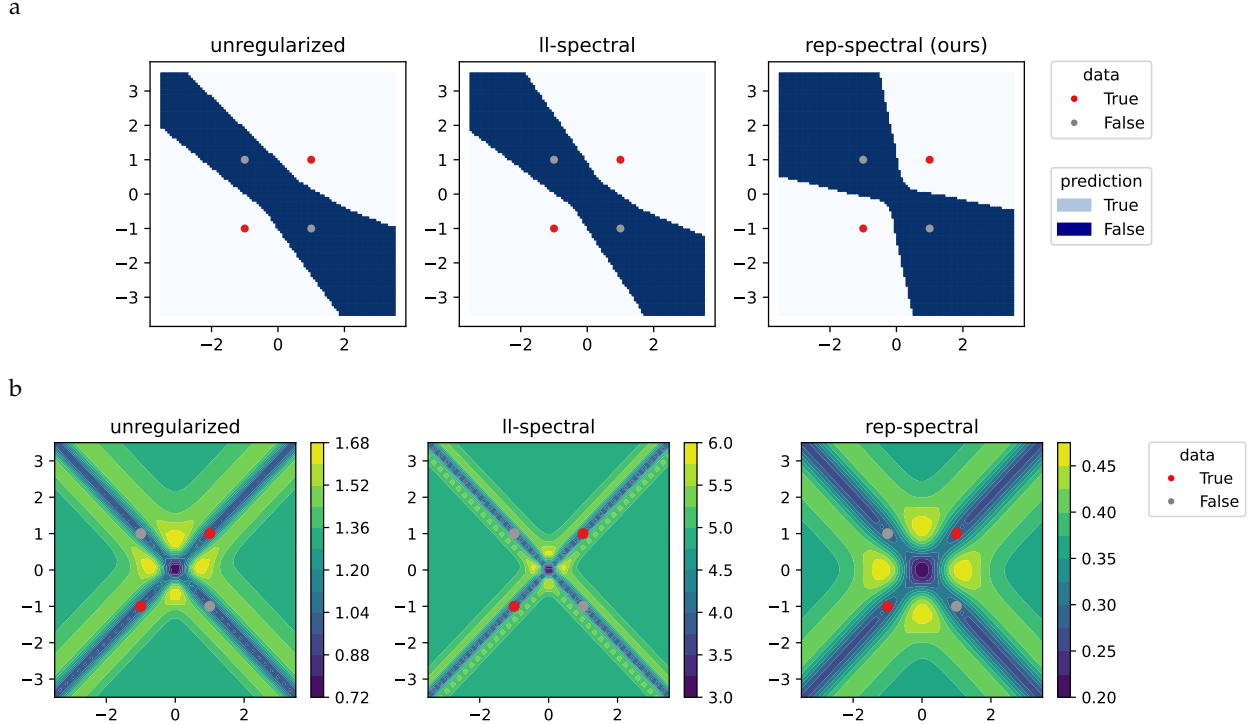


Figure 3: Effect of spectral regularization on the representations of MLPs trained on the toy XOR task. (a). Direct visualization of the decision boundaries of models trained using no regularization (*left*), l1-spectral regularization (*middle*), and our proposed rep-spectral regularization (*right*). The four training points are shown, colored according to their class. (b). Visualization of the volume element (see Remark 1), which measures the sensitivity of the representation to small variations in the input, for models trained with each of these three methods. For details, see Appendix E.1.

4.2 Shallow MLPs trained on MNIST images

We next apply our regularizer to single-hidden-layer MLPs trained to classify MNIST images [37], with flattened input of 784 dimensions and 2000 hidden units. We sample 1000 testing images and apply the TA algorithm to detect the minimum l_2 perturbation. In the fully supervised setting, though regularization slightly decreases test accuracy, we observe that excluding the last layer produces a smaller loss of accuracy and a larger increase in adversarial distance compared to regularizing all layers (Figure 4). We also visualize selected test images and their adversarial perturbations in Figure E.4 and observe an overall increase in scale of perturbation to make adversarial predictions compared to unregularized and spectral method. More training details and results are in Appendix E.1.

To test whether our regularizer leads to more robust representations, we discard the linear head and perform classification using multilogistic regression on the fixed feature representations (see Appendix E.1 for details). Surprisingly, in this setting our regularizer does not hurt test accuracy compared to the unregularized model (Figure 5). Moreover, the resulting model is more adversarially robust than when supervised pretraining of the representation is performed without regularization or with l1-spectral regularization (Figure 5). This suggests that, on a simple image classification task, our method achieves its stated goal: to enable representation learning that gives good adversarial robustness when an unregularized readout is trained to perform downstream tasks.

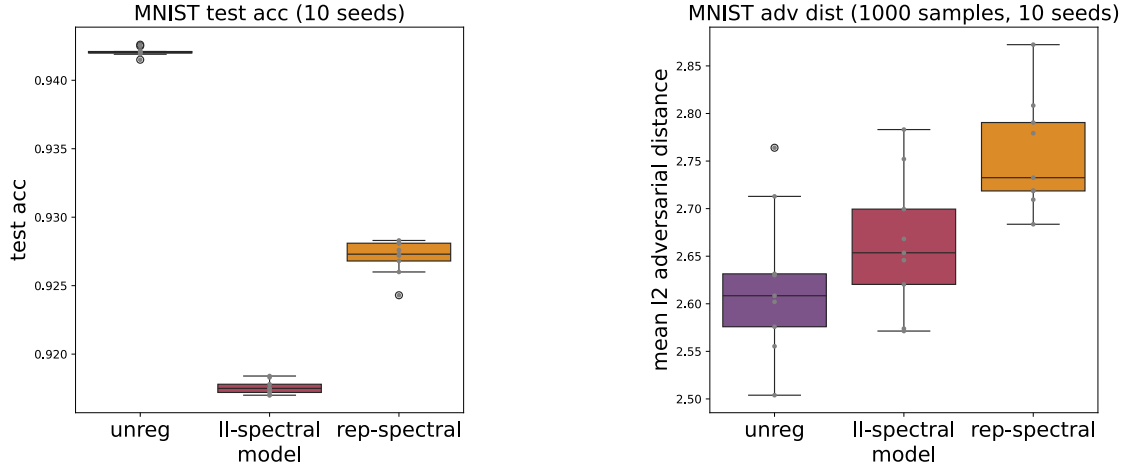


Figure 4: Spectral regularization during supervised training of a single-hidden-layer MLP on MNIST images improves robustness. For each regularization method, we show text accuracy (*left*) and adversarial distance averaged across 1000 samples (*right*) across 10 random seeds. Gray dots indicate the results for individual seeds, while boxplots show the mean and quartiles.

4.3 Deep Convolutional Networks: ResNet

As a final example in the supervised setting, we consider a deep convolutional architecture. We train ResNet18s [38] to classify CIFAR-10 images [39] using different adversarial regularization methods (see Appendix E.2 for training details). We plot the distribution of adversarial distances of 1000 randomly selected test samples in Figure 6a and test accuracy and average l2 adversarial distance in Figure 6b. As in Yoshida and Miyato [17]’s original proposal of l1-spectral regularization that incorporates the last layer, regularization provides a noticeable boost in test accuracy and robustness. Our rep-spectral method performs quite comparably to l1-spectral, with similar gains in test accuracy and perhaps marginally larger improvement in robustness. Interestingly, we see from the distributions of adversarial distance in Figure 6a that the gain in robustness over the unregularized model is mostly by enlarging the distances of samples that are originally close to the decision boundaries, as reflected by the suppression of the bump in the left tail of the density. See Figure E.5 for quantifying the distribution shift across different random seeds. This phenomenon is qualitatively consistent with our observations from the toy XOR task in Figure 3b.

4.4 Self-Supervised Learning: Barlow-Twins

We now turn at last to self-supervised pretraining, which provided the motivation for our work. As noted before, self-supervised learning (SSL) focuses on obtaining meaningful representations for various downstream applications without explicit label information. As all components of the network after the feature layer will be discarded in these downstream tasks, we naturally only regularize up to the feature layer. Here, we consider using the popular contrastive SSL method BarlowTwins [12] to learn representations of CIFAR-10, with a ResNet18 backbone. To evaluate accuracy and adversarial robustness on a downstream classification task, we train a multi-class logistic regression readout from the feature space. Full training details are provided in Appendix E.3. As we saw in supervised settings, pretraining with our rep-spectral regularizer yields a slight improvement in test accuracy and adversarial robustness (Figure 7). Though the gain in average adversarial robustness is not large (Figure 7b), by examining the distribution of adversarial distances we see that the robustness of the most vulnerable examples is improved (Figure 7a).

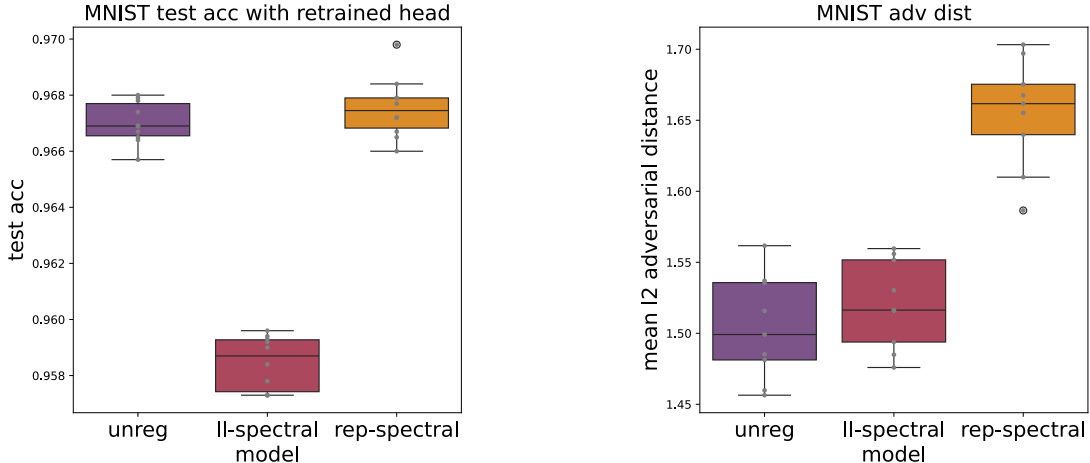


Figure 5: Re-training a readout from the hidden representation of an MLP pretrained on MNIST. For each regularization method, we show text accuracy (*left*) and adversarial distance averaged across 1000 samples (*right*) across 10 random seeds. Gray dots indicate the results for individual seeds, while boxplots show the mean and quartiles.

4.5 Transfer learning

Lastly, we apply our regularizer to transfer learning (TL) tasks. We pretrain ResNet50 on ImageNet-1K [40] and finetune on CIFAR-10 (see Appendix E.4 for details). In the finetuning stage, the readout layer is trained from scratch, while only miniscule adjustments are made to the hidden layers. For comparison in this setting, we add an additional candidate regularizer used at the finetuning stage, batch spectral shrinkage (BSS) [41]. We visualize the mean adversarial distances for 500 randomly test samples and report the mean over 10 random seeds in Figure 8 and corresponding test accuracy in Figure E.6. Although all model reaches 96% test accuracy consistently, they have dramatically different robustness level. We found adding rep-spectral regularization at the pretraining stage produces substantial gains in adversarial robustness, while adding adversarial regularization in the finetuning stage typically hurts adversarial robustness. The best robustness is obtained by adding our proposed regularizer during pretraining and then fine-tuning without regularization (compare the dark purple bar with the dark orange bar in Figure 8). A similar pattern holds in finetuning on other dataset such as Stanford Dog [42], Oxford Flowers [43], and MIT indoor [44]; see Appendix E.4 and Figure E.7 for more details. Therefore, our proposed method yields a substantial gain in robustness in a transfer learning setting.

5 Discussion

In this paper, we have shown that a simple regularization method encourages adversarial robustness during representation learning. We proved that the robustness of a representation is linked to the spectral norm of the input-wise Jacobian of the feature map (Lemma 1). Inspired by this bound, we proposed a regularizer that penalizes the top singular value of neural network layers only up to the feature space. Through ample experiments, we have shown that our regularizer is more effective than a previously-proposed method incorporating the readout layer in encouraging l_2 adversarial robustness during end-to-end training. This gain in robustness mostly results from increasing the adversarial distances to samples that are previously close to the decision boundaries (Figure 6a). The pattern holds in supervised, semi-supervised and transfer learning, including as training on synthetic data and MNIST using a shallow architecture, on CIFAR10 using ResNet18

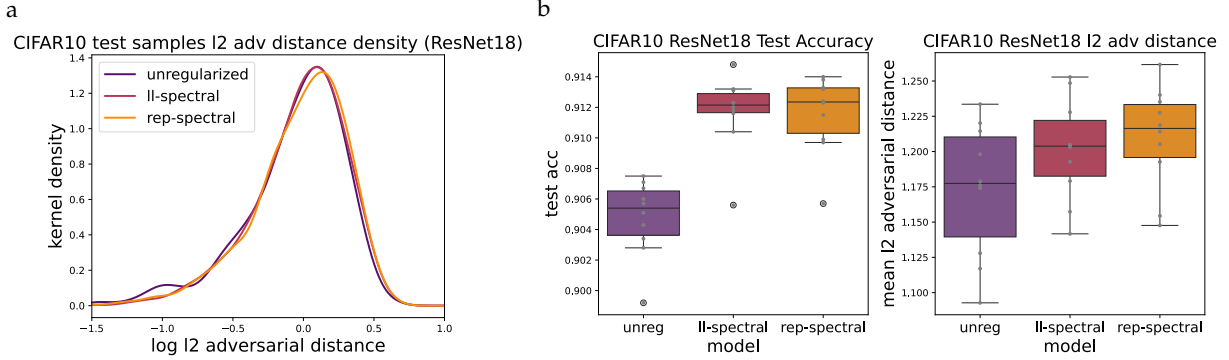


Figure 6: Spectral regularization during supervised training of ResNet18s to classify CIFAR-10 images improves accuracy and robustness. (a). Kernel density estimates of the distributions of adversarial distances across 1000 random samples for unregularized, l1-spectral, and rep-spectral models. Note that the distribution from rep-spectral shifts to the right of the distributions from unregularized and l1-spectral regularized models. (b). Test accuracy (*left*) and mean adversarial distance (*right*) for these models across 10 random seeds. Gray dots indicate the results for individual seeds, while boxplots show the mean and quartiles.

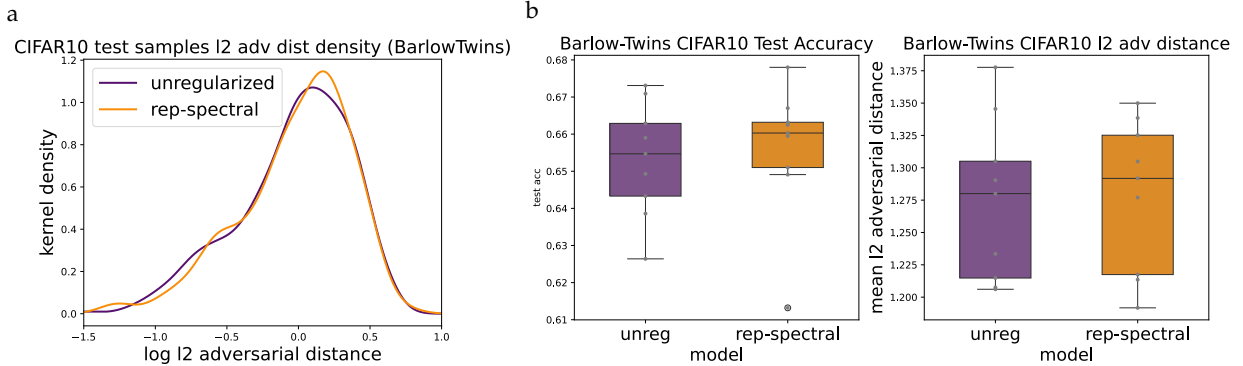


Figure 7: Spectral regularization during self-supervised BarlowTwins pretraining of a ResNet18 improves robustness of a readout in downstream classification. (a). Kernel density estimates of the distributions of adversarial distances across 1000 random samples for models pretrained without regularization and with rep-spectral regularization. (b). Test accuracy (*left*) and mean adversarial distance (*right*) for these models across 10 random seeds. Gray dots indicate the results for individual seeds, while boxplots show the mean and quartiles.

supervised training and BarlowTwins self-supervised training, and pretraining on ImageNet with subsequent finetuning on CIFAR10. In some experiments, we found that this new spectral regularizer even yields a gain in test accuracy.

Our proposed method is not without limitations. We observed limited improvement in robustness in self-supervised learning (Figure 7a), and saw that regularizing during the finetuning stage of transfer learning can decrease robustness (Figure 8). As our primary objective is to improve robustness of pretrained representations, the former limitation is more important. We note that adversarial robustness in SSL is in general not well-understood. It will be interesting to investigate whether there are ways to modify our training setup in which regularization yields substantial improvement in robustness. In particular, it will be interesting to investigate SSL pretraining using larger datasets, given the substantial improvements with representation quality observed with dataset scale in non-regularized settings [12–14].

This study opens the door for analyzing adversarial robustness on a per-layer basis. In deep networks, it is widely believed that early and later layers assume different roles in the learning

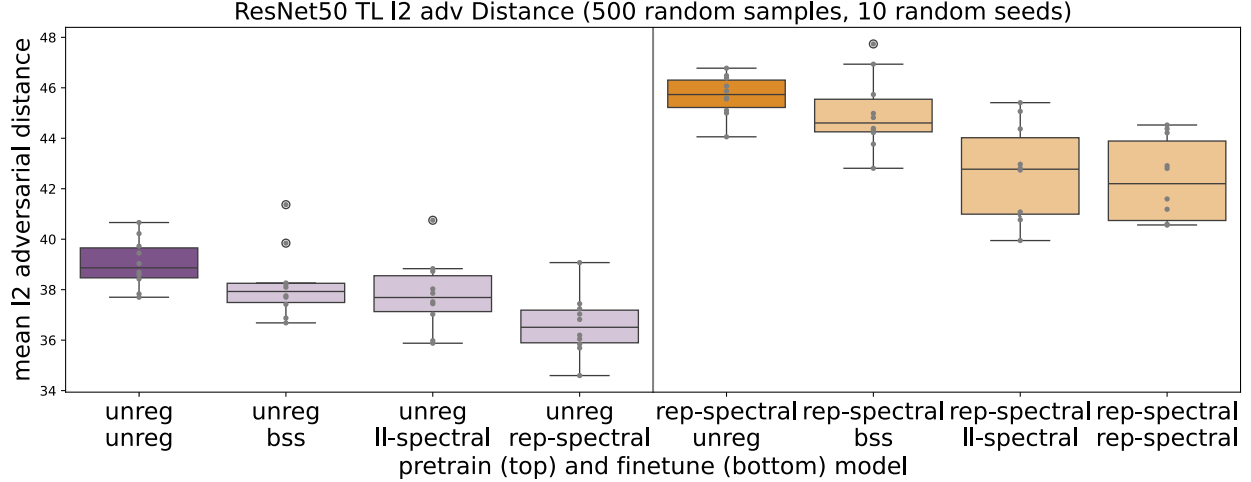


Figure 8: Mean Δ_x in transfer learning across different combinations of training schemes. The left half are finetuning from unregularized model, and the right half are finetuning from rep-spectral regularized model. In finetuning stage, adding additional regularization typically hurts adversarial robustness performance.

tasks. Early layers may be responsible for low-level feature extraction, while later layers adapt to high-level and task-specific features [34, 45, 46]. As analyzed in work by Dybala et al. [47] on the generalization performance of neural networks from a per-layer perspective, an interesting extension of our work would be to conduct ablation studies by turning on and off spectral regularizations for certain layers, not necessarily contiguous ones. This could allow one to identify the crucial layers contributing to model adversarial robustness.

It is also worth comparing our analysis with another line of adversarial robustness research based on adversarial training in the black-box attack literature [2, 3, 18, 48]. Adversarial training searches for adversarial samples after each parameter update and insert such samples into the training set, through which the adversarial robustness of the model is empirically injected. Although our method is data-independent and more parallel-computation-friendly, it is worth comprehensively comparing the runtime and adversarial robustness for adversarial attack methods and regularization methods that spontaneously provides adversarial robustness.

Acknowledgements

We thank Alexander Atanasov and Benjamin S. Ruben for helpful comments. JAZV and CP were supported by NSF Award DMS-2134157 and NSF CAREER Award IIS-2239780. CP is further supported by a Sloan Research Fellowship. This work has been made possible in part by a gift from the Chan Zuckerberg Initiative Foundation to establish the Kempner Institute for the Study of Natural and Artificial Intelligence.

References

- [1] Battista Biggio, Iginio Corona, Davide Maiorca, Blaine Nelson, Nedim Šrndić, Pavel Laskov, Giorgio Giacinto, and Fabio Roli. Evasion attacks against machine learning at test time. In *Machine Learning and Knowledge Discovery in Databases: European Conference, ECML PKDD 2013, Prague, Czech Republic, September 23–27, 2013, Proceedings, Part III 13*, pages 387–402. Springer, 2013.
- [2] Christian Szegedy, Wojciech Zaremba, Ilya Sutskever, Joan Bruna, Dumitru Erhan, Ian Goodfellow, and Rob Fergus. Intriguing properties of neural networks. *arXiv preprint arXiv:1312.6199*, 2013.
- [3] Ian J Goodfellow, Jonathon Shlens, and Christian Szegedy. Explaining and harnessing adversarial examples. *arXiv preprint arXiv:1412.6572*, 2014.
- [4] Xuanqing Liu, Yao Li, Chongruo Wu, and Cho-Jui Hsieh. Adv-bnn: Improved adversarial defense through robust bayesian neural network. In *International Conference on Learning Representations*, 2018.
- [5] Yao Li, Minhao Cheng, Cho-Jui Hsieh, and Thomas CM Lee. A review of adversarial attack and defense for classification methods. *The American Statistician*, 76(4):329–345, 2022.
- [6] Alexey Kurakin, Ian J Goodfellow, and Samy Bengio. Adversarial examples in the physical world. In *Artificial intelligence safety and security*, pages 99–112. Chapman and Hall/CRC, 2018.
- [7] Anish Athalye, Nicholas Carlini, and David Wagner. Obfuscated gradients give a false sense of security: Circumventing defenses to adversarial examples. In *International conference on machine learning*, pages 274–283. PMLR, 2018.
- [8] Aleksander Madry, Aleksandar Makelov, Ludwig Schmidt, Dimitris Tsipras, and Adrian Vladu. Towards deep learning models resistant to adversarial attacks. In *International Conference on Learning Representations*, 2018.
- [9] Ruiqi Gao, Tianle Cai, Haochuan Li, Cho-Jui Hsieh, Liwei Wang, and Jason D Lee. Convergence of adversarial training in overparametrized neural networks. *Advances in Neural Information Processing Systems*, 32, 2019.
- [10] Cihang Xie, Jianyu Wang, Zhishuai Zhang, Zhou Ren, and Alan Yuille. Mitigating adversarial effects through randomization. *arXiv preprint arXiv:1711.01991*, 2017.
- [11] Jeremy Cohen, Elan Rosenfeld, and Zico Kolter. Certified adversarial robustness via randomized smoothing. In *international conference on machine learning*, pages 1310–1320. PMLR, 2019.
- [12] Jure Zbontar, Li Jing, Ishan Misra, Yann LeCun, and Stéphane Deny. Barlow twins: Self-supervised learning via redundancy reduction. In *International conference on machine learning*, pages 12310–12320. PMLR, 2021.
- [13] Ting Chen, Simon Kornblith, Mohammad Norouzi, and Geoffrey Hinton. A simple framework for contrastive learning of visual representations. In Hal Daumé III and Aarti Singh, editors, *Proceedings of the 37th International Conference on Machine Learning*, volume 119 of *Proceedings of Machine Learning Research*, pages 1597–1607. PMLR, 13–18 Jul 2020. URL <https://proceedings.mlr.press/v119/chen20j.html>.
- [14] Alec Radford, Jong Wook Kim, Chris Hallacy, Aditya Ramesh, Gabriel Goh, Sandhini Agarwal, Girish Sastry, Amanda Askell, Pamela Mishkin, Jack Clark, Gretchen Krueger, and Ilya Sutskever. Learning transferable visual models from natural language supervision. In Marina Meila and Tong Zhang, editors, *Proceedings of the 38th International Conference on Machine Learning*, volume 139 of *Proceedings of Machine Learning Research*, pages 8748–8763. PMLR, 18–24 Jul 2021. URL <https://proceedings.mlr.press/v139/radford21a.html>.
- [15] Danny Hernandez, Jared Kaplan, Tom Henighan, and Sam McCandlish. Scaling laws for transfer. *arXiv*, 2021.
- [16] Matthias Hein and Maksym Andriushchenko. Formal guarantees on the robustness of a classifier against adversarial manipulation. *Advances in neural information processing systems*, 30, 2017.
- [17] Yuichi Yoshida and Takeru Miyato. Spectral norm regularization for improving the generalizability of deep learning. *arXiv preprint arXiv:1705.10941*, 2017.
- [18] Tao Bai, Jinqi Luo, Jun Zhao, Bihan Wen, and Qian Wang. Recent advances in adversarial training for adversarial robustness. *arXiv preprint arXiv:2102.01356*, 2021.

- [19] Shengchao Liu, Dimitris Papailiopoulos, and Dimitris Achlioptas. Bad global minima exist and sgd can reach them. *Advances in Neural Information Processing Systems*, 33:8543–8552, 2020.
- [20] Dimitris Bertsimas and Jack Dunn. *Machine learning under a modern optimization lens*. Dynamic Ideas LLC Charlestown, MA, 2019.
- [21] Dimitris Bertsimas and Dick den Hertog. Robust and adaptive optimization. (*No Title*), 2022.
- [22] Arjun Nitin Bhagoji, Daniel Cullina, and Prateek Mittal. Lower bounds on adversarial robustness from optimal transport. *Advances in Neural Information Processing Systems*, 32, 2019.
- [23] Elvis Dohmatob. Classifier-independent lower-bounds for adversarial robustness. *arXiv preprint arXiv:2006.09989*, 2020.
- [24] Wieland Brendel, Jonas Rauber, and Matthias Bethge. Decision-based adversarial attacks: Reliable attacks against black-box machine learning models. *arXiv preprint arXiv:1712.04248*, 2017.
- [25] Jianbo Chen, Michael I Jordan, and Martin J Wainwright. Hopskipjumpattack: A query-efficient decision-based attack. In *2020 IEEE Symposium on Security and Privacy (SP)*, pages 1277–1294. IEEE, 2020.
- [26] Huichen Li, Xiaojun Xu, Xiaolu Zhang, Shuang Yang, and Bo Li. Qeba: Query-efficient boundary-based blackbox attack. In *Proceedings of the IEEE/CVF conference on computer vision and pattern recognition*, pages 1221–1230, 2020.
- [27] Yujia Liu, Seyed-Mohsen Moosavi-Dezfooli, and Pascal Frossard. A geometry-inspired decision-based attack. In *Proceedings of the IEEE/CVF International Conference on Computer Vision*, pages 4890–4898, 2019.
- [28] Ziang Yan, Yiwen Guo, Jian Liang, and Changshui Zhang. Policy-driven attack: Learning to query for hard-label black-box adversarial examples. In *International Conference on Learning Representations*, 2020.
- [29] Chen Ma, Xiangyu Guo, Li Chen, Jun-Hai Yong, and Yisen Wang. Finding optimal tangent points for reducing distortions of hard-label attacks. *Advances in Neural Information Processing Systems*, 34:19288–19300, 2021.
- [30] Md Farhamdur Reza, Ali Rahmati, Tianfu Wu, and Huaiyu Dai. Cgba: Curvature-aware geometric black-box attack. In *Proceedings of the IEEE/CVF International Conference on Computer Vision*, pages 124–133, 2023.
- [31] Hongyang Zhang, Yaodong Yu, Jiantao Jiao, Eric Xing, Laurent El Ghaoui, and Michael Jordan. Theoretically principled trade-off between robustness and accuracy. In *International conference on machine learning*, pages 7472–7482. PMLR, 2019.
- [32] Aditi Raghunathan, Sang Michael Xie, Fanny Yang, John Duchi, and Percy Liang. Understanding and mitigating the tradeoff between robustness and accuracy. *arXiv preprint arXiv:2002.10716*, 2020.
- [33] Judy Hoffman, Daniel A. Roberts, and Sho Yaida. Robust learning with jacobian regularization. *arXiv*, 2019.
- [34] Jacob A Zavatone-Veth, Sheng Yang, Julian A Rubinfeld, and Cengiz Pehlevan. Neural networks learn to magnify areas near decision boundaries. *arXiv preprint arXiv:2301.11375*, 2023.
- [35] Hanie Sedghi, Vineet Gupta, and Philip M Long. The singular values of convolutional layers. *arXiv preprint arXiv:1805.10408*, 2018.
- [36] Alexandra Senderovich, Ekaterina Bulatova, Anton Obukhov, and Maxim Rakhuba. Towards practical control of singular values of convolutional layers. *Advances in Neural Information Processing Systems*, 35:10918–10930, 2022.
- [37] Yann LeCun, Corinna Cortes, and CJ Burges. MNIST handwritten digit database. *ATT Labs [Online]*, 2, 2010. URL <http://yann.lecun.com/exdb/mnist>.
- [38] Kaiming He, Xiangyu Zhang, Shaoqing Ren, and Jian Sun. Deep residual learning for image recognition. In *Proceedings of the IEEE conference on computer vision and pattern recognition*, pages 770–778, 2016.
- [39] Alex Krizhevsky. Learning multiple layers of features from tiny images. Technical report, University of Toronto, 2009. URL <https://www.cs.toronto.edu/~kriz/cifar.html>.

- [40] Jia Deng, Wei Dong, Richard Socher, Li-Jia Li, Kai Li, and Li Fei-Fei. Imagenet: A large-scale hierarchical image database. In *2009 IEEE conference on computer vision and pattern recognition*, pages 248–255. Ieee, 2009.
- [41] Xinyang Chen, Sinan Wang, Bo Fu, Mingsheng Long, and Jianmin Wang. Catastrophic forgetting meets negative transfer: Batch spectral shrinkage for safe transfer learning. *Advances in Neural Information Processing Systems*, 32, 2019.
- [42] Aditya Khosla, Nityananda Jayadevaprakash, Bangpeng Yao, and Li Fei-Fei. Novel dataset for fine-grained image categorization. In *First Workshop on Fine-Grained Visual Categorization, IEEE Conference on Computer Vision and Pattern Recognition*, Colorado Springs, CO, June 2011.
- [43] Maria-Elena Nilsback and Andrew Zisserman. Automated flower classification over a large number of classes. In *Indian Conference on Computer Vision, Graphics and Image Processing*, Dec 2008.
- [44] Ariadna Quattoni and Antonio Torralba. Recognizing indoor scenes. In *2009 IEEE conference on computer vision and pattern recognition*, pages 413–420. IEEE, 2009.
- [45] Nick Cammarata, Shan Carter, Gabriel Goh, Chris Olah, Michael Petrov, Ludwig Schubert, Chelsea Voss, Ben Egan, and Swee Kiat Lim. Thread: Circuits. *Distill*, 2020. doi: 10.23915/distill.00024. <https://distill.pub/2020/circuits>.
- [46] Jenelle Feather, Guillaume Leclerc, Aleksander Mądry, and Josh H. McDermott. Model metamers reveal divergent invariances between biological and artificial neural networks. *Nature Neuroscience*, 26(11):2017–2034, Nov 2023. ISSN 1546-1726. doi: 10.1038/s41593-023-01442-0. URL <https://doi.org/10.1038/s41593-023-01442-0>.
- [47] Luciano Dyballa, Evan Gerritz, and Steven W Zucker. A separability-based approach to quantifying generalization: which layer is best? *arXiv preprint arXiv:2405.01524*, 2024.
- [48] Florian Tramèr, Alexey Kurakin, Nicolas Papernot, Ian Goodfellow, Dan Boneh, and Patrick McDaniel. Ensemble adversarial training: Attacks and defenses. *arXiv preprint arXiv:1705.07204*, 2017.
- [49] Vignesh Kothapalli. Neural collapse: A review on modelling principles and generalization. *Transactions on Machine Learning Research*, 2023.
- [50] Vardan Papyan, X. Y. Han, and David L. Donoho. Prevalence of neural collapse during the terminal phase of deep learning training. *Proceedings of the National Academy of Sciences*, 117(40):24652–24663, 2020. doi: 10.1073/pnas.2015509117. URL <https://www.pnas.org/doi/abs/10.1073/pnas.2015509117>.
- [51] Jianfeng Lu and Stefan Steinerberger. Neural collapse under cross-entropy loss. *Applied and Computational Harmonic Analysis*, 59:224–241, 2022. ISSN 1063-5203. doi: <https://doi.org/10.1016/j.acha.2021.12.011>. URL <https://www.sciencedirect.com/science/article/pii/S1063520321001123>. Special Issue on Harmonic Analysis and Machine Learning.
- [52] Hugo Touvron, Andrea Vedaldi, Matthijs Douze, and Hervé Jégou. Fixing the train-test resolution discrepancy. In *Advances in Neural Information Processing Systems (NeurIPS)*, 2019.
- [53] Charles R. Harris, K. Jarrod Millman, Stéfan J van der Walt, Ralf Gommers, Pauli Virtanen, David Cournapeau, Eric Wieser, Julian Taylor, Sebastian Berg, Nathaniel J. Smith, Robert Kern, Matti Picus, Stephan Hoyer, Marten H. van Kerkwijk, Matthew Brett, Allan Haldane, Jaime Fernández del Río, Mark Wiebe, Pearu Peterson, Pierre Gérard-Marchant, Kevin Sheppard, Tyler Reddy, Warren Weckesser, Hameer Abbasi, Christoph Gohlke, and Travis E. Oliphant. Array programming with NumPy. *Nature*, 585:357–362, 2020. doi: 10.1038/s41586-020-2649-2.
- [54] J. D. Hunter. Matplotlib: A 2d graphics environment. *Computing in Science & Engineering*, 9(3):90–95, 2007. doi: 10.1109/MCSE.2007.55.
- [55] Wes McKinney et al. Data structures for statistical computing in python. In *Proceedings of the 9th Python in Science Conference*, volume 445, pages 51–56. Austin, TX, 2010.
- [56] F. Pedregosa, G. Varoquaux, A. Gramfort, V. Michel, B. Thirion, O. Grisel, M. Blondel, P. Prettenhofer, R. Weiss, V. Dubourg, J. Vanderplas, A. Passos, D. Cournapeau, M. Brucher, M. Perrot, and E. Duchesnay. Scikit-learn: Machine learning in Python. *Journal of Machine Learning Research*, 12:2825–2830, 2011.

- [57] Adam Paszke, Sam Gross, Francisco Massa, Adam Lerer, James Bradbury, Gregory Chanan, Trevor Killeen, Zeming Lin, Natalia Gimelshein, Luca Antiga, Alban Desmaison, Andreas Kopf, Edward Yang, Zachary DeVito, Martin Raison, Alykhan Tejani, Sasank Chilamkurthy, Benoit Steiner, Lu Fang, Junjie Bai, and Soumith Chintala. Pytorch: An imperative style, high-performance deep learning library. In H. Wallach, H. Larochelle, A. Beygelzimer, F. d'Alché-Buc, E. Fox, and R. Garnett, editors, *Advances in Neural Information Processing Systems*, volume 32. Curran Associates, Inc., 2019. URL https://proceedings.neurips.cc/paper_files/paper/2019/file/bdbca288fee7f92f2bfa9f7012727740-Paper.pdf.

A Proofs and Discussions

A.1 Proof of Lemma 1

We first restate the lemma using dual norm formulation.

Restatement of Lemma 1 Suppose a neural network classifier $F : \mathbb{R}^n \rightarrow \mathbb{R}^K$ is continuously differentiable and can be decomposed as in Equation (2). Suppose $x \in \mathbb{R}^n$ is a sample input belonging to class c and $\delta \in \mathbb{R}^n$ an adversarial perturbation to x with error class predicted as k . Further, given $\frac{1}{p} + \frac{1}{q} = 1$, assume $\|\delta\|_p \leq R$ for some radius $R > 0$, we have

$$\|\delta_x\|_p \geq \frac{\left(W_c^{(L)} - W_k^{(L)}\right) \Phi(x) + b_c^{(L)} - b_k^{(L)}}{\|W_c^{(L)} - W_k^{(L)}\|_q} \cdot \frac{1}{\max_{y \in B_p(x, R)} \|\nabla \Phi(y)\|_q} \quad (\text{A.1})$$

where $f(z) = W^{(L)}z + b^{(L)}$ is the last layer linear transformation, $W_c^{(L)}$ is the c -th row of $W^{(L)}$ treated as a row vector, and $\nabla \Phi(\cdot)$ is the Jacobian of the feature map w.r.t. input.

Proof. This lemma directly extends the main theorem presented in [16], where a general classifier was considered instead.

Define $h = f \circ \Phi$. First, $F(x)$ and $h(x)$ have the same ordering of its coordinates, since SoftMax is a strictly monotonic transformation. More explicitly,

$$F_c(x + \delta) \leq F_k(x + \delta) \iff h_c(x + \delta) \leq h_k(x + \delta) \quad (\text{A.2})$$

second, by Taylor expansion to the first order in integral form, we have

$$h_k(x + \delta) = h_k(x) + \int_0^1 \langle \nabla h_k(x + t\delta), \delta \rangle dt, \quad \forall k \in [K] \quad (\text{A.3})$$

where $\nabla h_k(\cdot)$ is the gradient taken w.r.t. to the input, not the parameter of the neural network. Applying Equation (A.3) to Equation (A.2) on both sides, we have

$$h_c(x) - h_k(x) \leq \int_0^1 \langle \nabla h_k(x + t\delta) - \nabla h_c(x + t\delta), \delta \rangle dt \quad (\text{A.4})$$

$$\leq \|\delta\|_p \int_0^1 \|\nabla h_k(x + t\delta) - \nabla h_c(x + t\delta)\|_q dt \quad (\text{Hölder with } \frac{1}{p} + \frac{1}{q} = 1) \quad (\text{A.5})$$

$$\leq \|\delta\|_p \cdot \max_{y \in B_p(x, R)} \|\nabla h_k(y) - \nabla h_c(y)\|_q \quad (R \text{ the norm of } \delta) \quad (\text{A.6})$$

$$\leq \|\delta\|_p \cdot \max_{y \in B_p(x, R)} \|\nabla \Phi(y)\|_q \|\nabla f_k(\Phi(y)) - \nabla f_c(\Phi(y))\|_q \quad (\text{Chain Rule}) \quad (\text{A.7})$$

here we use $\|\cdot\|_q$ to denote the vector-induced matrix norm when the input is a matrix. Using Equation (A.7), rearranging terms, we get

$$\|\delta\|_p \geq \frac{h_c(x) - h_k(x)}{\max_{y \in B_p(x, R)} \|\nabla \Phi(y)\|_q \|\nabla f_k(\dots) - \nabla f_c(\dots)\|_q} \quad (\text{A.8})$$

note that we explicitly drop the dependence of ∇f on its input since f is assumed linear. Parametrizing $f(\cdot)$ by $W^{(L)}, b^{(L)}$ and use the fact that $h = f \circ \Phi$, we get Equation (A.1). Lastly, taking $p = q = 2$ and assuming centered data, we get Equation (3). \square

A.2 Derivation of Feature Regularization

In this section we derive the regularization presented in Equation (5). Consider an explicit parameterization of $F(·; \Theta)$ as a neural network with only linear layers parametrized by $\Theta = \{W^{(1)}, b^{(1)}, \dots, W^{(L)}, b^{(L)}\}$ and non-linear activation function $\phi(·)$ and denote z^l as the l -th layer preactivation value and $D^{(l)}$ a diagonal matrix with diagonals given by $\text{diag}(D^{(l)}) = \phi'(z^{(l)})$, then

$$\nabla \Phi(x) = D^{(L-1)} W^{(L-1)} D^{(L-2)} W^{(L-2)} \dots D^{(1)} W^{(1)} \quad (\text{A.9})$$

therefore

$$\lambda_{\max}(g) = \lambda_{\max}(D^{(L-1)} W^{(L-1)} \dots D^{(1)} W^{(1)} (W^{(1)})^T (D^{(1)})^T \dots (W^{(L-1)})^T (D^{(L-1)})^T) \quad (\text{A.10})$$

$$\leq \prod_{l=1}^{L-1} \lambda_{\max}(W^{(l)} (W^{(l)})^T) \cdot \lambda_{\max}(D^{(l)} (D^{(l)})^T) \quad (\text{A.11})$$

where the last line uses the cyclic property in computing the eigenvalues recursively. Note that for common activation function the derivatives are upper-bounded by 1, and so $\lambda_{\max}(D^{(l)} (D^{(l)})^T)$ is upper bounded by 1. We have

$$\lambda_{\max}(g) \leq \prod_{l=1}^{L-1} \lambda_{\max}(W^{(l)} (W^{(l)})^T) = \prod_{l=1}^{L-1} \sigma_{\max}^2(W^{(l)}) \quad (\text{A.12})$$

where σ_{\max} is the largest singular value. This motivates Equation (5) by replacing the product by a sum for easier back propagation.

A.3 Tracking θ_x with fixed representations

In this section we comment on the dynamics of θ_x when we fix the neural representations. Under simplifying assumptions, we can analytically compute the last layer alignment and thus θ_x here.

Kothapalli [49] showed that in deep neural network the representation can demonstrate a neural collapse (NC) phenomenon where the representations form a simplex equiangular tight frame (ETF) (see also the original work by Pappas et al. [50], and theoretical work by Lu and Steinerberger [51]). That is, data of the same class are sent to the same place with unit norm in the feature space and data from different class are maximally distant from each other. Assuming the ETF layout, we can analytically derive the last layer alignment under certain conditions. We present the following lemma.

Lemma 2. *Suppose that we have K samples in the dataset and each with a different class. In this K -class classification with feature space \mathbb{R}^d with $d > K$, assuming that representations $\{z_k\}_{k=1}^K$ reach an ETF layout, with small random Gaussian initialization for the last layer $f(z) : \mathbb{R}^d \rightarrow \mathbb{R}^K : z \rightarrow Wz$, gradient descent on the last layer only aligns weight vectors W_k , the k -th row of W , with the neural representations of the sample from k -th class.*

Proof. Since we only have K samples and each comes from a different class, a full-batch gradient descent has the following cross entropy loss:

$$L(W) = \frac{1}{K} \sum_{k=1}^K \log \left(1 + \sum_{l \neq k} e^{(W_l - W_k) z_k} \right) \quad (\text{A.13})$$

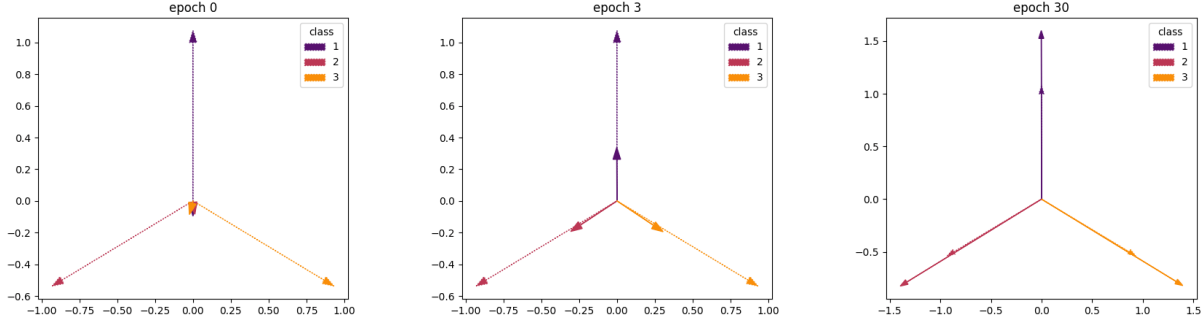


Figure A.1: Last Layer Alignment with std = 0.001 initialization

Define the composition of last layer linear map with the Softmax operation as $g = \text{Softmax} \circ f$. The gradient descent direction for each row of W can be thus given by

$$-\frac{\partial L}{\partial W_k} = \frac{1}{K} \left[\left(\sum_{l \neq k} g_l(z_k) \right) z_k - \sum_{l \neq k} g_k(z_l) z_l \right] \quad (\text{A.14})$$

where g_k is the k -th output of g . Using small initialization we have $g(x_k) \approx [\frac{1}{K}, \frac{1}{K}, \dots, \frac{1}{K}]$ close to a uniform distribution for all $k \in [K]$. This suggests that at the first step, the descent direction is given by

$$-\frac{\partial L}{\partial W_k} \approx \frac{K-1}{K^2} z_k - \frac{1}{K^2} \sum_{l \neq k} z_l = \frac{1}{K} z_k \quad (\text{A.15})$$

where in the last step we use $\sum_{l \neq k} z_l = -z_k$, since in an ETF layout we have $\sum_{k=1}^K z_k = 0$.

We may then repeat the analysis for subsequent steps. We no longer have uniform output values for each data sample, but $g_l(z_k), \forall l \neq k$ would be roughly equal by symmetry and small, so that the descent direction continues to pull W_k towards z_k albeit with a smaller strength. \square

We demonstrate this prediction in a toy 2D task: suppose 3 samples in 2 dimensions are of different classes and they form a simplex ETF layout. This means they are on the unit circle and are exactly 120 degrees away from each other. Starting with Gaussian initialization, the last layer vectors gradually align with the representation vectors under a full-batch gradient descent training with learning rate 0.01. We demonstrate the alignment process for small initialization (std=0.001) in Figure A.1 and large initialization (std=0.1) in Figure A.2.

We could extend the results to arbitrary number of data samples with balanced class label distributions as well. With the same assumptions, we can write down θ_x in simple cases.

Lemma 3. *With the same assumption in Lemma 2, and suppose x belongs to class c with representation z_c and z_k is one feature representation from any other class, we have*

$$\theta_x \approx \frac{1 - z_k^T z_c}{\|z_c - z_k\|_2} \quad (\text{A.16})$$

whose value is the same for all $k \neq c$ due to the symmetry in the ETF layout.

Proof. Using Lemma 2, $W_k \approx c z_k, c > 0$, with the same scalar c for all class k . Plugging in the definition of θ_x we get Equation (A.16). \square

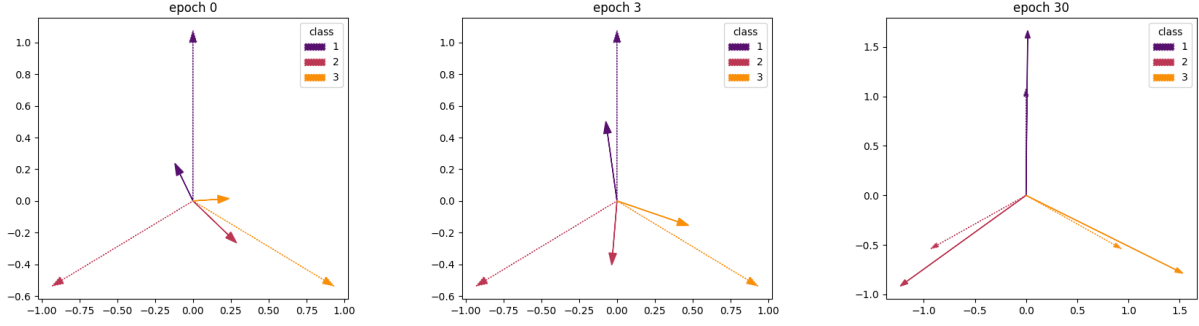


Figure A.2: Last Layer Alignment with std = 0.1 initialization

If we relax the ETF layout assumption, one may still write down the gradient and analytically track the gradient flow and get expressions of W_k at convergence, but in that case W_k do not align with z_k due to a lack of symmetry in the feature representations, and subsequently θ_x for different classes will be different.

A.4 Tracking θ_x and $\|\Phi(x)\|_2$ during joint training

In general, if we jointly train feature representation and last layer, we do not have the nice analytic prediction as in Lemma 2 and Lemma 3. We could still empirically track the two quantities. In simple cases we see that compared to initialization, both $\|\phi(x)\|_2$ and θ_x expand when training with cross entropy loss. See Figure A.3 for cross entropy loss training on 2D XOR dataset and Figure A.4 for MNIST data. This solidifies our argument that from a feature representation perspective, to bump the lower bound on adversarial robustness, one would like to control the $\|\nabla\Phi(\cdot)\|_2$ term.

B Linearization of a Multi-channel Convolution Layer

This section provides a brief description of the linearization of multi-channel convolution layer and subsequently getting the maximum eigenvalue of this linear operation. More details and proofs can be found in [35, 36].

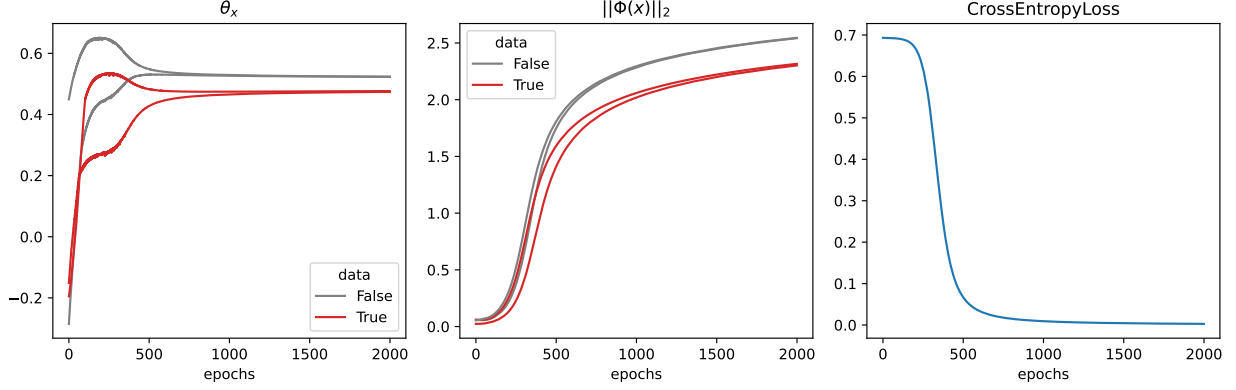
B.1 Construction of the linear map $\tilde{\mathcal{K}}$

A periodic 2D convolution operation can be considered a linear transformation on the vectorized input, and the weights are constructed from the filters. Consider $X \in \mathbb{R}^{c_{in} \times n \times n}$ an input image to a convolution layer with c_{in} numbers of input channels and height/width given by n . A multichannel filter $\mathcal{K} \in \mathbb{R}^{c_{out} \times c_{in} \times k \times k}$ with stride s with c_{out} number of output channels and kernel size k can be rewritten into a matrix $\tilde{\mathcal{K}} \in \mathbb{R}^{c_{out} n_{out}^2 \times c_{in} n^2}$ such that

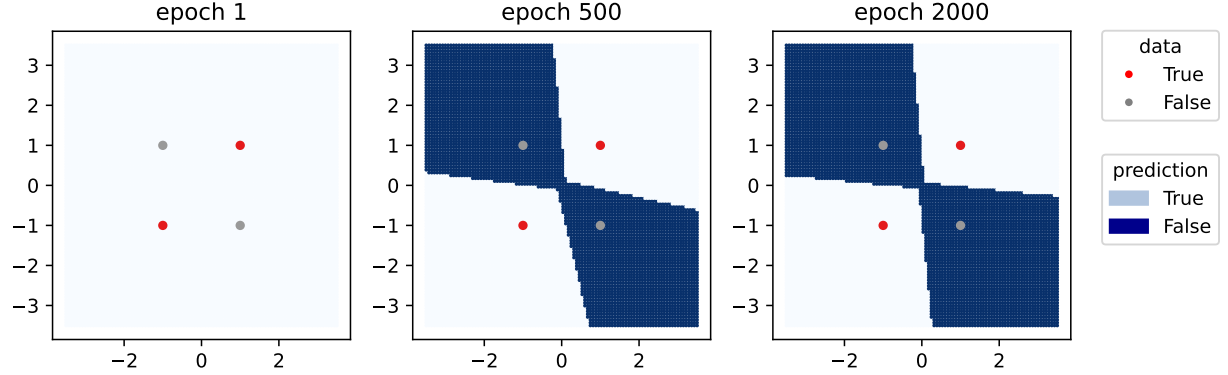
$$\text{Vec}(\text{Conv2D}(X)) = \tilde{\mathcal{K}} \text{Vec}(X) \quad (\text{B.1})$$

where $\text{Vec}(\cdot)$ is a row-major reshaping of X (i.e. the default behavior of calling `.flatten()` in NumPy and PyTorch), and n_{out} the output height/width given by $n_{out} = \lfloor \frac{n-1}{s} + 1 \rfloor$.

The transformation $\tilde{\mathcal{K}}$ consists of $n^2 \times n^2$ blocks of doubly circulant matrix, and each of the doubly circulant matrix contains data that come from appropriately slicing the zero-padded filter \mathcal{K} that matches with the same shape of the 2D input image. It could be validated that the singular



a θ_x , $\|\Phi(x)\|_2$, and cross entropy loss over the course of training



b Snapshot of decision boundary at different training epochs

Figure A.3: In this simple example, we train XOR task on a single-hidden-layer neural network with 20 hidden units using full batch gradient descent and Gaussian initialization with zero mean and 0.01 std. Compared to initialization, θ_x increased and $\|\Phi(x)\|_2$ expanded over the course of training.

values of $\tilde{\mathcal{K}}$ is the union of all singular values of 2D FFT-transformed blocks of the appropriate slicing, so that to compute the top singular value of $\tilde{\mathcal{K}}$, one does not need to construct $\tilde{\mathcal{K}}$ itself but instead should record the top singular values of FFT-transformed slices and take the max of all these maximum singular values, which saves substantial computational resources.

In Code Block 1 we present PyTorch code that is modified from theorem 2 of [36] for computing the square of top singular value of $\tilde{\mathcal{K}}$.

B.2 Speeding Up Top Eigenvalue Computation: Power Iteration Across Parameter Updates

Since here we are only interested in the maximal eigenvalue, we could use batched power iteration (algorithm described in Appendix C) to jointly compute the top eigenvalues only for 2D FFT-transformed blocks. Both 2D FFT transformation and batch eigenvalue update are GPU friendly. Furthermore, since between consecutive parameter updates, the change in filter map is likely small, iterations in the power method can be amortized across parameter updates. We empirically find that the outcome of conducting a batch power iteration update to the top eigenvalues every 20 parameter updates have little difference in performance compared to computing the exact eigenvalue before each parameter update. See Appendix E.2 for the results.

The amortization across parameter update or across epochs trick has been noticed previously

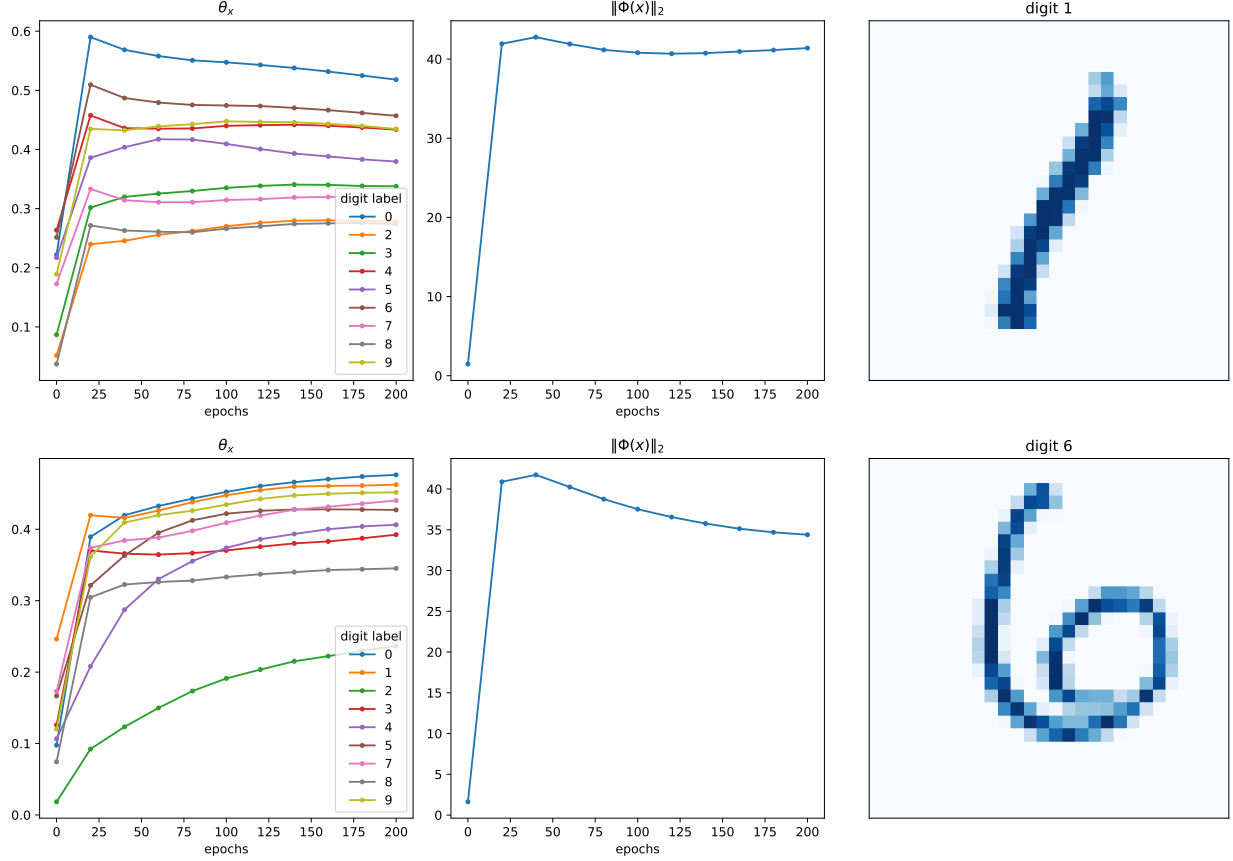


Figure A.4: θ_x , $\|\Phi(x)\|_2$ for a test sample of class 1 (top panel) and class 6 (bottom panel). In MNIST setting with small initialization (gaussian mean 0 std 0.01) and normal cross entropy loss training, we observe expansion of θ_x and $\|\Phi(x)\|_2$ over training.

in Yoshida and Miyato [17], but was only applied to fully-connected layers.

B.3 Implication of the Dependence on Input Dimension

Although a 2D convolution operator applies to images with arbitrary size and channels, the top singular value of the linearized map depends on the size and channels. To impose spectral regularization to convolution layers, it is thus recommended to use the size and channels of the test images for regularization. The impact of regularizing on one set of images and testing on another with different shapes and channels remains to be explored.

C Power Iteration to Compute the Top Singular Value of a Linear Map

Power iteration is an iterative algorithm to compute the eigenspectrum of a diagonalizable matrix. We can extend the algorithm to compute the largest singular value of a complex-valued matrix. The algorithm is described in Algorithm 1. In practice, $N = 1$ is enough, since the parameter moves slowly as we train the cross entropy classification loss.

D Finding Adversarial Distances by Tangent Attack [29]

The Tangent Attack algorithm proposed by Ma et al. [29] provides a good heuristic for finding adversarial distances in the black-box setting. Here, we briefly sketch how this algorithm operates; we refer the reader to [29] for details.

Given a correctly classified sample x , we initialize the algorithm by adding a fixed number of Gaussian perturbations with predetermined standard deviations that adapts to the input dimension. Among all perturbed samples, we keep ones that were classified differently by the neural network classifier and select the one with the minimum l_2 distance to the original sample x . We then run a binary search along the line segment from x to that sample to locate a point that is on the decision boundary. We call this point x_0 as our initial guess to the adversarial sample to x .

Next we iteratively shrink the distance between $x_t, t \in \{0, 1, \dots, T\}$ and x , where T is a predefined maximum number of updates to the adversarial guesses so that at the end of the algorithm x_T is considered the adversarial sample to x and the adversarial distance $\delta_x = \|x_T - x\|_2$. The update is done by performing the following three key steps in sequence: at each $t \in \{0, 1, \dots, T - 1\}$

1. **estimate a normal direction** to the decision boundary, pointing to the adversarial region: we take local perturbation to x_t . Based on the prediction on these perturbations, averaging the vectors that give adversarial prediction gives us an estimate to the normal direction;
2. **find the tangent point** in the 2D plane generated by x, x_t , and the normal direction. construct a hemisphere in the direction of the normal vector with a predefined small radius, find the tangent plane to the hemisphere that passes through x and locate the tangent point k . This step is done by analytic geometry and a closed form update can be analytically derived.
3. **conduct a binary search** along the line segment from x to k , get a sample on the decision boundary and assign that to x_{t+1} . In this way, x_{t+1} is a valid adversarial sample with a different prediction from x but is closer to x than x_t .

In our experiments, we use $T = 40$ throughout. Other hyperparameters such as the radius of hemisphere and the number of local perturbations for normal direction estimation follows identically from the hemisphere implementation in [29].

E Experiment Details

Code to reproduce all experiments is freely available on GitHub.² All experiments in this paper were run on the Harvard FASRC Cannon cluster supported, using NVIDIA A100 40GB GPUs. Experiments reported in the main text required less than 240 GPU-hours.

Our code base is adapted from various publicly available ones, including TangentAttack³ with an Apache V2 license for evaluating the adversarial distances, FixRes[52]⁴ with a CC BY-NC 4.0 license for multi-GPU training Resnet50, SimCLR⁵ with an MIT license for SimCLR model data loading and evaluation, BarlowTwins⁶ with an MIT license for BarlowTwins data loading and evaluation, practical_svd_conv⁷ with a BSD-3-Clause license for efficient computations of top

²<https://github.com/Pehlevan-Group/rep-spectral>

³<https://github.com/machanic/TangentAttack>

⁴<https://github.com/facebookresearch/FixRes>

⁵<https://github.com/sthalles/SimCLR>

⁶<https://github.com/facebookresearch/barlowtwins/tree/main>

⁷https://github.com/WhiteTeaDragon/practical_svd_conv

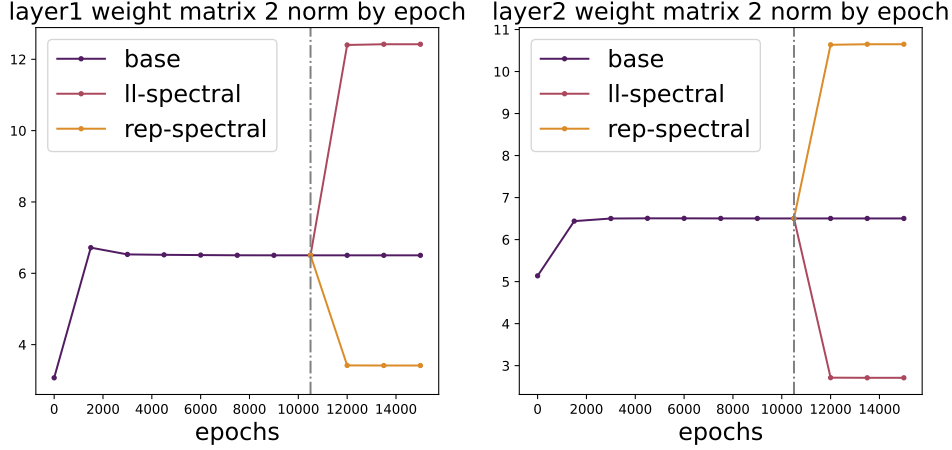


Figure E.1: l1-spectral regularization and rep-spectral regularization weight norm change over training clean XOR data shown in Figure 3a. At epoch 10500 we turn on the adversarial regularization, before which there is only crossentropy loss.

singular value of 2D convolution layers, and lastly `nn_curvature`⁸ with an MIT license for volume element computations.

Our Python code also uses some common publicly available packages, including NumPy [53] with a BSD license, Matplotlib [54] with a BSD license, Pandas [55] under a BSD license, scikit-learn [56] with a BSD license, PyTorch [57] under a modified BSD license, tqdm with an MIT license, and toml with an MIT license.

Data used in the project include MNIST [37], CIFAR-10 [39], ImageNet-1K [40], Stanford Dog [42], Oxford Flowers [43], and MIT indoor [44].

E.1 Shallow Network

To train shallow network for clean and noisy XOR with 8 hidden units, we train for 15000 epochs using full batch GD with 1.0 learning rate, 0.9 momentum, zero or 1e-4 weight decay, the same regularization strength ($\gamma = 0.0001$), and a regularization burnin period of 10500 epochs (70% unregularized training + 30% regularized training), all models could classify all 4 points correctly but demonstrate vastly different decision landscapes.

For shallow network, there are only two connection layers. The difference between Yoshida and Miyato [17]’s l1-spectral regularization and our rep-spectral regularization is heuristically most pronounced in this case, since here rep-spectral is regularizing only half of the layers that l1-spectral is regularizing.

In clean XOR training, by plotting the matrix 2-norm of the connection weights in each layer through respective regularization, we found a striking contrast between the two. By imposing the same regularization strength for rep-spectral and l1-spectral, rep-spectral is able to control effectively the weight norm of the feature layer with an expansion of weight norm in the last layer; l1-spectral regularization is the exact opposite that it fails to control the weight norm in the feature layer. This is shown in the Figure E.1.

In settings where the last layer is discarded and retrained such as transfer and self-supervised learning, rep-spectral method is preferred due to its attention to feature layer weight norm rather than just the last layer.

⁸https://github.com/Pehlevan-Group/nn_curvature

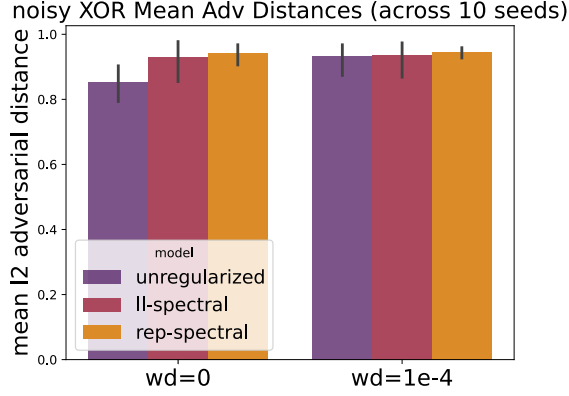


Figure E.2: average Δ_x found by TA across 10 different seed for clean XOR (left) and noisy XOR (right) with and without weight decay of $1e-4$. The error bar shows plus and minus one standard deviation across 10 seeds around the mean. This behavior is consistent across 10 different random seeds

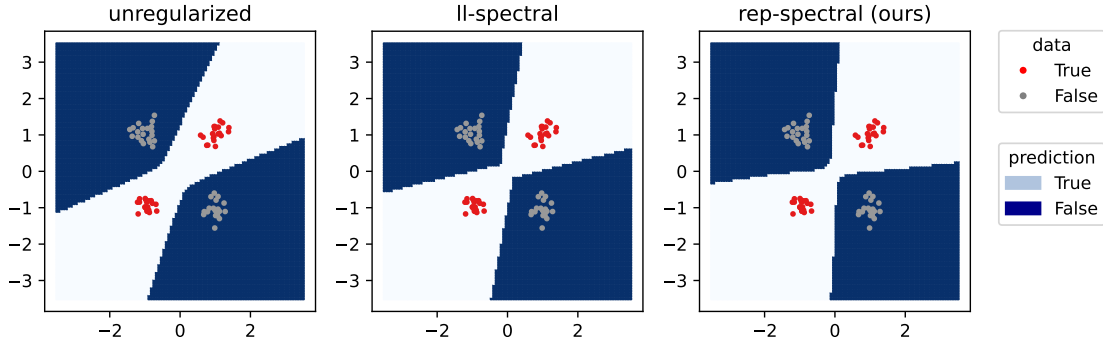


Figure E.3: Noisy XOR decision boundaries

To train shallow network with 784 hidden units on MNIST dataset, we train for 200 epochs using SGD with batch size 1024, learning rate 0.1, momentum 0.9, weight decay $1e-4$, $\gamma = 0.001$, and a regularization burn-in period of 160 epochs (80% unregularized training + 20% regularized training). The update of the eigen directions are done through one power iteration every parameter update.

To testify the robustness of representations, we retrain a new linear head using multilogistic regression with a l_2 regularization parameter 1 (i.e. the default setting when applying `sklearn.linear_model.LogisticRegression`) trained on the feature representations of the same train samples. To make decision of a test sample, we get the feature representation through the feature map and then apply multilogistic regression trained to get decisions.

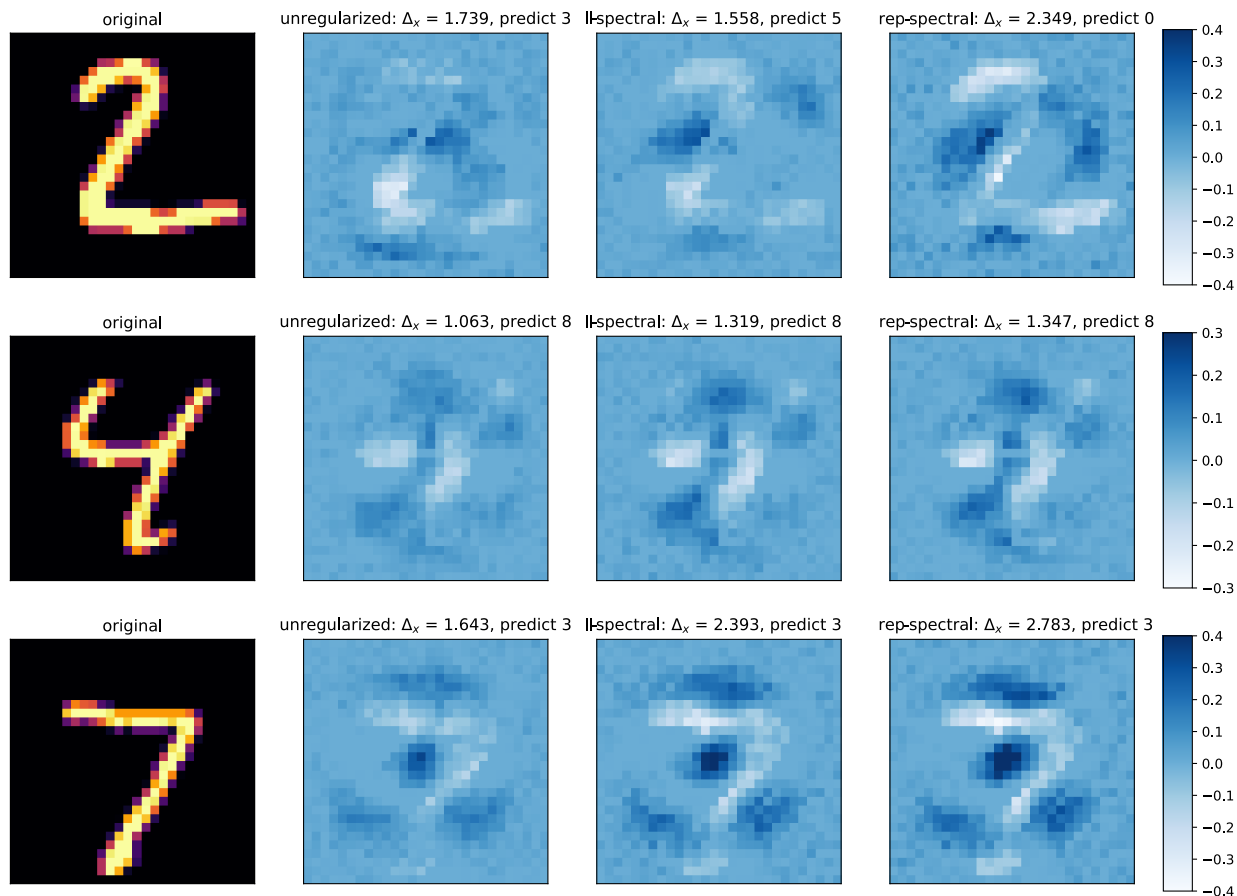


Figure E.4: MNIST Test Images and the perturbation δ_x found by Tangent Attack [29] for three methods. The adversarial distances Δ_x and the adversarial predictions are reported on the titles. In general, our method encourages larger adversarial distances compared to other methods.

E.2 Deep Convolutional Networks

We train for 200 epochs using SGD with batch size 1024, learning rate 0.01, momentum 0.9, weight decay $1e-4$, $\gamma = 0.01$, and an adversarial regularization burnin period of 160 epochs (80% unregularized training + 20% regularized training). To alleviate regularization computational cost, we only update the eigenvector direction using the power iteration once every 24 parameter updates.

E.3 Self-Supervised Learning

In BarlowTwins training, using ResNet18, we train on CIFAR10 using SGD for 1000 epochs with learning rate 0.01, momentum 0.9, weight decay $1e-4$, $\gamma = 0.01$, and a regularization burnin period of 900 epochs (90% unregularized training + 10% regularized training). Likewise, to alleviate training cost, we amortize power iteration to perform once every 24 parameter updates.

E.4 Transfer Learning

In unregularized pretraining, we train ResNet50 for 120 epochs using SGD with learning rate 0.02, momentum 0.9, weight decay $1e-4$, linear scheduling 30 epochs with decay 0.1. We distribute

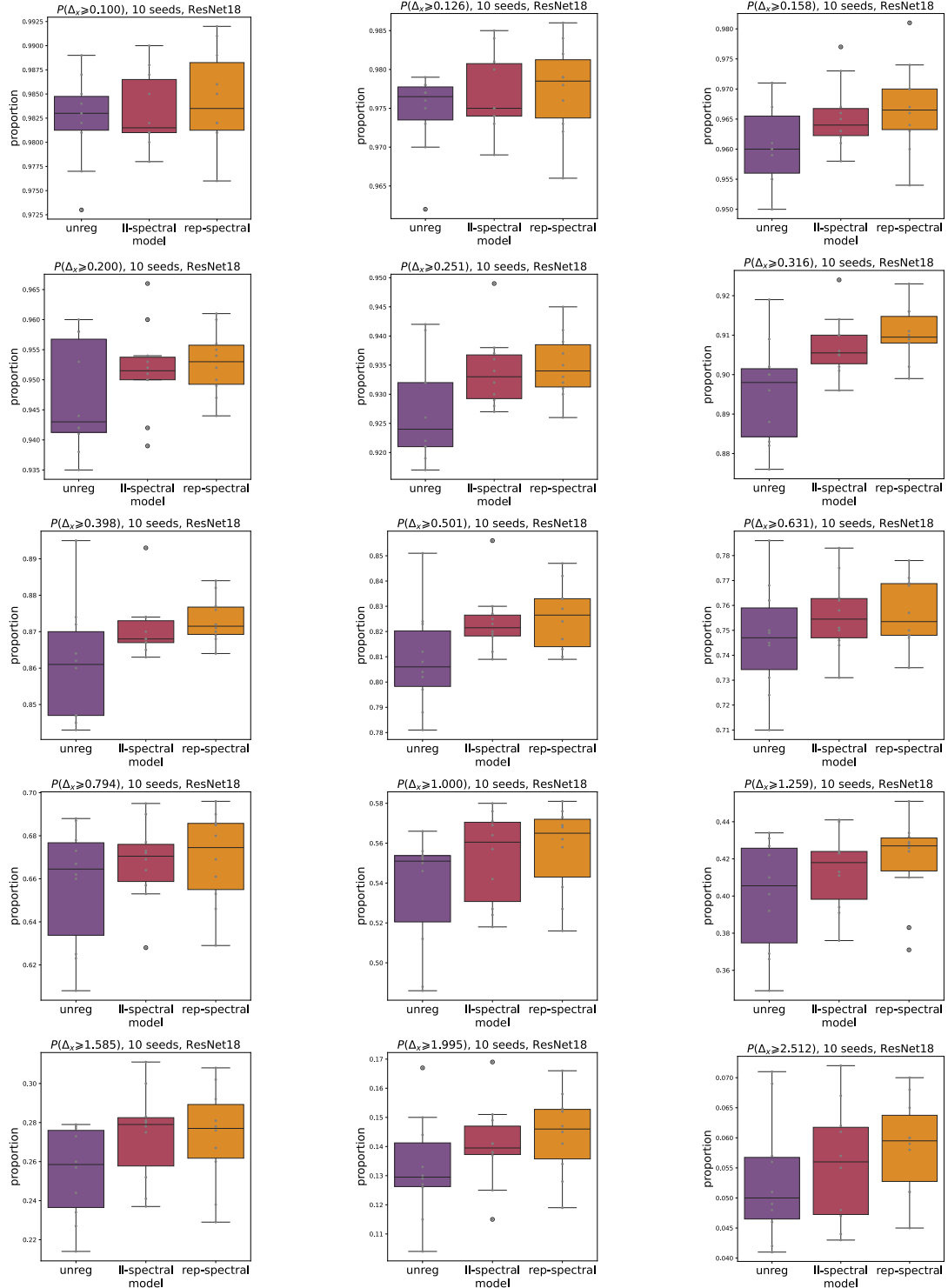


Figure E.5: Proportion of 1000 randomly selected samples with adversarial distance larger than a threshold across 10 different seeds in training ResNet18s on CIFAR10, with the individual proportions colored in grey. 15 thresholds are displayed in increasing order. Higher proportion means better adversarial robustness. Across all thresholds, rep-spectral achieves the highest proportion.

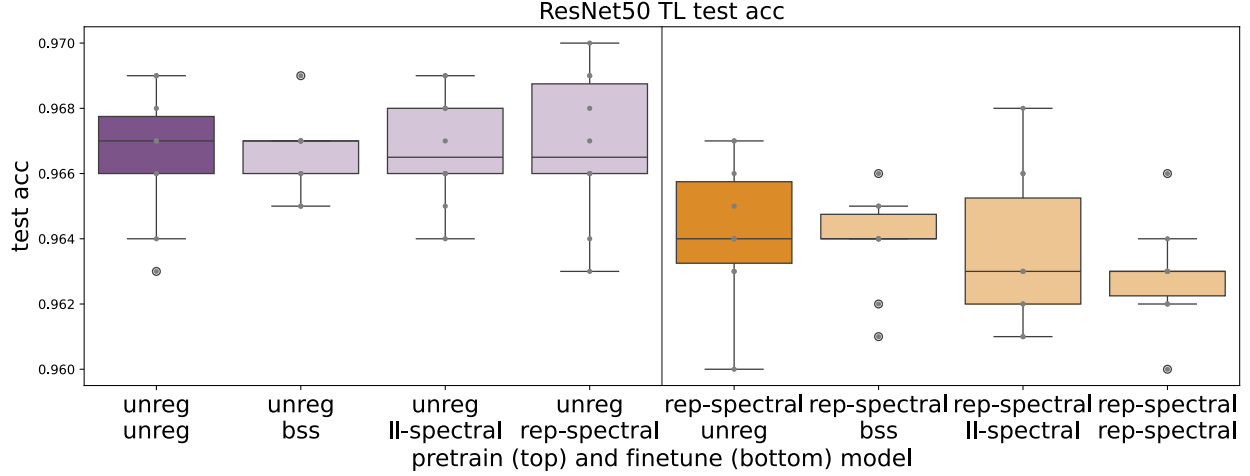


Figure E.6: Test accuracy in transfer learning across multiple combinations of training schemes. The left half are finetuning from unregularized model, and the right half are finetuning from rep-spectral regularized model. All models reach an accuracy level of 96%, but have different adversarial robustness level shown in Figure 8.

batchsize of 512 images across 4 GPUs for training. For regularized pretraining, starting at epoch 80 (67% unregularized training + 33% regularized training), we turn on rep-spectral regularization with $\gamma = 0.001$, with power update of top eigenvectors every 160 parameter updates to alleviate computation costs.

We test these two models' performance at finetune time, in which we train on CIFAR10 scale to 224 by 224 images with the same dimensionality with ImageNet for 50 epochs using SGD with 0.01 learning rate on linear head and 0.002 learning rate for the backbone, each with a CosineAnnealing scheduling with max parameter 200 epochs for both backbone and linear head. We visualize the test accuracy for each model of each random seed in Figure E.6. On average, finetuned model starting with regularized weights have 0.2% drop in test accuracy than the ones starting with unregularized weights.

We also tested performance on more commonly used transfer learning target datasets: Stanford Dog [42] contains images of 120 different kinds of dogs; Oxford Flowers [43] contains images of 102 different types of flowers; MIT Indoor [44] contains indoor scenes of 67 different categories. Three dataset have the same input dimensionality with ImageNet1k. Similar as in finetuning on CIFAR10, we the model pretrained on ImageNet either with or without our regularizations, and in the finetuning stage we perform normal CrossEntropy optimization. As different target dataset have different inherent complexity, we finetune on the three models using different set of hyperparameters. To finetune on Stanford dog, we train for 50 epochs using SGD with a learning rate 0.005 for last layer and 0.001 for the feature layers; to finetune on Oxford Flowers we train for 1000 epochs using SGD with a learning rate 0.005 for last layer and 0.001 for the feature layer; and to finetune on MIT Indoor, we train for 100 epochs using SGD with a learning rate 0.01 and 0.002 for the feature layers. All dataset are trained with a batchsize of 64. With either pretrained weights with or without regularization, we repeat each training for 5 times and report the end test accuracy and adversarial distances in Figure E.7. Although finetuned models starting from regularized weights have 2% drop in test accuracy compared to the finetuned models starting with unregularized weights, we have roughly 10% increase in mean adversarial distances across different dataset, suggesting that our feature map trained is not uniquely robust to finetuning on one particular dataset.

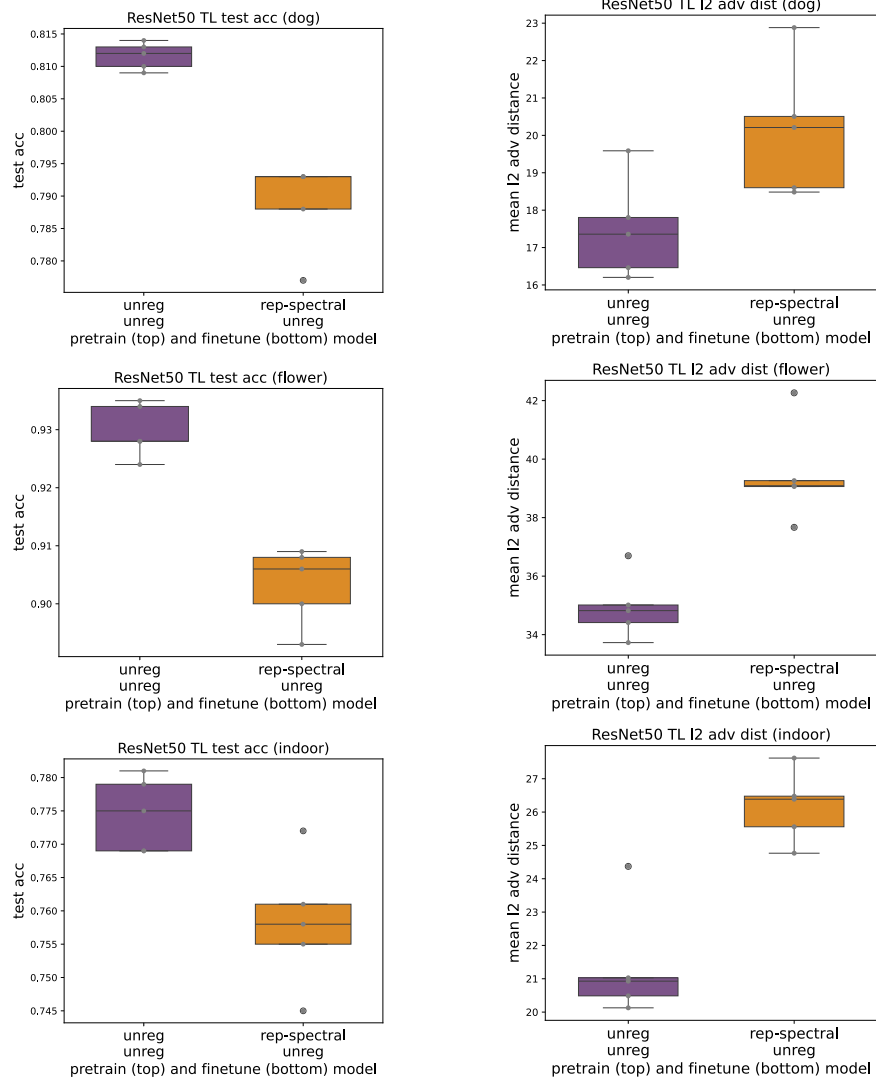


Figure E.7: Test accuracy and mean adversarial distances from pretraining on ImageNet and finetuning on Stanford Dog (top row), Oxford Flowers (middle row), MIT Indoor (bottom row). The grey dots indicate the value from each of the 5 random seeds. Sacrificing at most 2% of test accuracy, we obtain at least 10% gain in the adversarial distances on average.

```

# import packages
import torch
from torch.nn.functional import pad

# function body
def get_multi_channel_top_eigval_with_stride(
    kernel: torch.Tensor, h: int, w: int, stride: int
) -> torch.Tensor:
    """
    compute top eigen value of a convolution layer
    * code tested only for even n and stride = 1 or 2.

    :param kernel: the conv2d kernel, with shape (c_out, c_in, k, k)
    :param h: the image height
    :param w: the image width
    :param stride: the stride of convolution
    :return the top singular value for conv layer
    """
    # pad zeros to the kernel to make the same shape as input
    c_out, c_in, k_h, k_w = kernel.shape
    pad_height = h - k_h
    pad_width = w - k_w
    kernel_pad = pad(kernel, (0, pad_height, 0, pad_width), mode="constant", value=0)
    str_shape_height, str_shape_width = h // stride, w // stride

    # downsample the kernel
    transforms = torch.zeros(
        (c_out, c_in, stride**2, str_shape_height, str_shape_width)
    ).to(kernel.device)
    for i in range(stride):
        for j in range(stride):
            transforms[:, :, i * stride + j, :, :] = kernel_pad[
                :, :, i::stride, j::stride
            ]

    # batch fft2
    transforms = torch.fft.fft2(transforms)
    transforms = transforms.reshape(c_out, -1, str_shape_height, str_shape_width)

    # reorg (h // stride, w // stride, c_out, c_in * stride^2)
    P = transforms.permute(2, 3, 0, 1)

    # compute singular value squared
    # by computing eigenvalues of  $KK^T$  or  $K^TK$ , whichever is faster
    eigvals = torch.linalg.eigvalsh(
        torch.einsum("...ij,...kj->...ik", torch.conj(P), P)
    )
    if P.shape[3] > P.shape[2]:
        else torch.einsum("...ji,...jk->...ik", torch.conj(P), P)
    )

    # keep top eigenvalue only
    top_eig = eigvals.max()
    return top_eig

```

Code Block 1: Python code for computing the top singular value of the operator form of a convolutional layer

Algorithm 1 Power Iteration for Top Singular Value Squared

Require: $M \in \mathbb{C}^{m \times n}, N \in \mathbb{N}$

▸ N number of iterations

Ensure: $\lambda = \sigma_1(M)^2$

$v = v_0$

▸ Randomly Generated or from previous training iterates

$v \leftarrow \frac{v}{\|v\|_2}$

▸ Normalize

$i \leftarrow 0$

while $i < N$ **do**

$u \leftarrow Mv$

$u \leftarrow \frac{u}{\|u\|_2}$

$v \leftarrow M^*u$

▸ Conjugate Transpose

$v \leftarrow \frac{v}{\|v\|_2}$

$i \leftarrow i + 1$

end while

$p = Mv$

▸ $Mv_1 = \sigma_1 u_1$

$\lambda = \|p\|_2^2$
